Geochimica et Cosmochimica Acta xxx (xxxx) xxx

Contents lists available at ScienceDirect

Geochimica et Cosmochimica Acta

journal homepage: www.elsevier.com/locate/gca

Tracing early disk substructures and accretionary relationships through nitrogen isotopes in iron meteorites

Evelyn Füri [a,*], Fridolin Spitzer [b], Julie Gamblin [a], Christoph Burkhardt [b], Béatrice Luais [a], Julien Boulliung [a], Laurent Zimmermann [a]

[a] Université de Lorraine, CNRS, CRPG, F-54000 Nancy, France
[b] Max Planck Institute for Solar System Research, Justus-von-Liebig-Weg 3, 37077 Göttingen, Germany

ARTICLE INFO

Associate editor: Eric Quirico

Keywords:
Nitrogen
Noble gases
Iron meteorites
Noble gas mass spectrometry
Ammonia ice line
Disk substructures

ABSTRACT

Iron meteorites provide key insights into the formation conditions of planetesimals in the early protoplanetary disk. To investigate the sources of nitrogen (N) in non-carbonaceous (NC) and carbonaceous (CC) iron meteorite parent bodies—and to trace the spatiotemporal N isotopic heterogeneity in the inner and outer disk—we present combined N–Ne–Ar isotopic data for 14 irons from the under-studied IIAB-IIG and IID groups, and 14 ungrouped irons of either NC or CC heritage. These measurements, obtained via CO_2 laser heating and multi-collection noble gas mass spectrometry, allow us to exclude contributions from solar gases and cosmogenic ^{15}N. New data for two comparatively N-rich IIG irons confirm a genetic link with the IIAB group, supporting the view that NC magmatic iron meteorite groups are characterized by low $\delta^{15}N$ values (–90 to –80 ‰). These results suggest that NC iron meteorite parent bodies accreted a smaller proportion of ^{15}N-rich (organic) carriers than later-formed chondritic bodies, possibly due to thermal processing at the tar line. Two NC ungrouped magmatic irons have markedly higher $\delta^{15}N$ values (–2.0 ‰ and +9.1 ‰); however, their Ge-depleted compositions raise uncertainty as to whether these signatures reflect primary, parent-body-specific characteristics or result from secondary volatile loss. In contrast, CC magmatic irons, including the IID group and CC ungrouped irons, predominantly record positive $\delta^{15}N$ values. Among these, the N isotopic compositions of three CC ungrouped irons—New Baltimore (+104 ‰), Hammond (+112 ‰), and La Caille (+206 ‰)—resemble those of IIC irons and Renazzo-type (CR) carbonaceous chondrites, reinforcing their genetic link to the IIC/CR reservoir, where ammonia ice was likely an important N carrier. This implies that an isotopically CR-like, ammonia-rich reservoir was established in the outer protoplanetary disk during the earliest stages of its evolution and persisted for several million years. Taken together, these findings indicate that the primary N isotopic composition of differentiated and undifferentiated planetesimals was governed by the local mixture of isotopically distinct N-bearing phases, itself shaped by evolving condensation and evaporation fronts in the early protoplanetary disk.

1. Introduction

Chondrites have long served as key archives for tracing spatial nitrogen (N) isotope heterogeneity in the early protoplanetary disk. Their N isotopic compositions, typically reported as $\delta^{15}N$ values (the per mil (‰) deviation from the atmospheric $^{15}N/^{14}N$ ratio of 0.003676; Nier, 1950), differ markedly from that of the protosolar nebula (Marty et al., 2011; Füri and Marty, 2015), and reflect contributions from both isotopically light and heavy N-bearing components (e.g., Kerridge, 1985; Grady and Wright, 2003). Notably, $\delta^{15}N$ values largely overlap between non-carbonaceous (NC) chondrites, whose parent bodies accreted in the inner disk, and carbonaceous (CC) chondrites, whose parent bodies are generally thought to have formed farther out (see Bermingham et al., 2020; Broadley et al., 2022, for recent reviews) (Fig. 1**b**). Distinctly elevated $\delta^{15}N$ values are restricted to (i) Bencubbin-type (CB) and high-metal (CH) carbonaceous chondrites (not shown in Fig. 1), whose presumed late formation in an impact-generated vapor plume (Krot et al., 2005; Florin et al., 2021; Desch et al., 2023) severely complicates the interpretation of their N isotopic signatures (e.g., Marty et al., 2010), and (ii) late-formed Renazzo-type (CR) carbonaceous chondrites (Kung and Clayton, 1978; Robert and Epstein, 1982; Grady et al., 1983; Pearson et al., 2006; Alexander et al., 2012, 2013), which

* Corresponding author at: Centre de Recherches Pétrographiques et Géochimiques (CRPG), 15 rue Notre Dame des Pauvres, 54500 Vandœuvre-les Nancy, France.
E-mail address: evelyn.furi@univ-lorraine.fr (E. Füri).

https://doi.org/10.1016/j.gca.2026.05.037
Received 18 September 2025; Accepted 30 May 2026
Available online 2 June 2026
0016-7037/© 2026 The Author(s). Published by Elsevier Ltd. This is an open access article under the CC BY license (http://creativecommons.org/licenses/by/4.0/).

may contain material sourced from the outermost disk regions, beyond the ammonia ice line (Sridhar et al., 2021; Van Kooten et al., 2024; Hewins et al., 2025). Thus, although some N isotopic heterogeneity is observed, N in chondrites does not show a NC-CC isotopic dichotomy analogous to that observed in elements with nucleosynthetic anomalies (e.g., Cr, Ti; Trinquier et al., 2007, 2009; Warren, 2011). This distribution challenges the notion of spatially distinct N reservoirs in the inner and outer disk—at least at the time of chondrite parent body accretion. However, because these undifferentiated bodies formed relatively late, ~1.8 to 4 Myr after calcium-aluminum-rich inclusions (CAIs) (Bouvier et al., 2025, and references therein), their isotopic signatures may not capture the full range of N isotopic variability present during the earliest stages of disk evolution and planetary accretion.

'Magmatic' iron meteorites, composed primarily of Fe-Ni alloy crystals, are remnants of the metallic cores of the earliest-formed, differentiated planetesimals (Scott, 1972; Scott and Wasson, 1975). Distinct chemical trends, along with isotopic evidence, divide magmatic iron meteorites into separate groups, indicating they originate from ten different planetesimal cores (Wasson, 1967, 1969, 1970; Wasson and Kimbeblin, 1967; Scott and Wasson, 1975; Wasson and Choe, 2009; Anand et al., 2024). In contrast, the number of parent bodies sampled by the 'non-magmatic' or 'silicate-bearing' iron meteorites is less certain, as their origins may involve partial differentiation and/or impact-induced melting and mixing (Mittlefehldt et al., 1998; Benedix et al., 2000, 2013; Luais, 2007). Ungrouped irons, which include both magmatic and non-magmatic members, presumably represent fragments of at least 50 distinct, poorly sampled planetesimals (Scott, 2020).

Iron meteorites conform to the bimodal nucleosynthetic isotope anomaly distribution observed in chondrites and silicate achondrites. Several groups (magmatic IC, IIAB-IIG, IIIAB, IIIE, and IVA irons, as well as the non-magmatic IAB and IIE irons) have NC-like Mo-Ru-Ni isotopic signatures, whereas others (IIC, IID, IIF, IIIF, and IVB irons) have CC-like signatures (Burkhardt et al., 2011; Budde et al., 2016; Kruijer et al., 2017; Bermingham et al., 2018; Nanne et al., 2019; Spitzer et al., 2020). Recent Mo isotope analyses have revealed that the NC-CC dichotomy also extends to the large number of planetesimals sampled by ungrouped irons (Spitzer et al., 2025a). These findings suggest that the parent bodies of iron meteorites accreted at two distinct radial locations within the protoplanetary disk, likely sunward and beyond Jupiter's orbit. Importantly, the parent bodies of NC and CC iron meteorites accreted contemporaneously within the first ~ 1 Myr of Solar System history, as inferred from Hf–W model ages and thermal modeling of planetesimals internally heated by ^{26}Al decay (Kruijer et al., 2017; Spitzer et al., 2021, Spitzer et al., 2025a; Bryson et al., 2026).

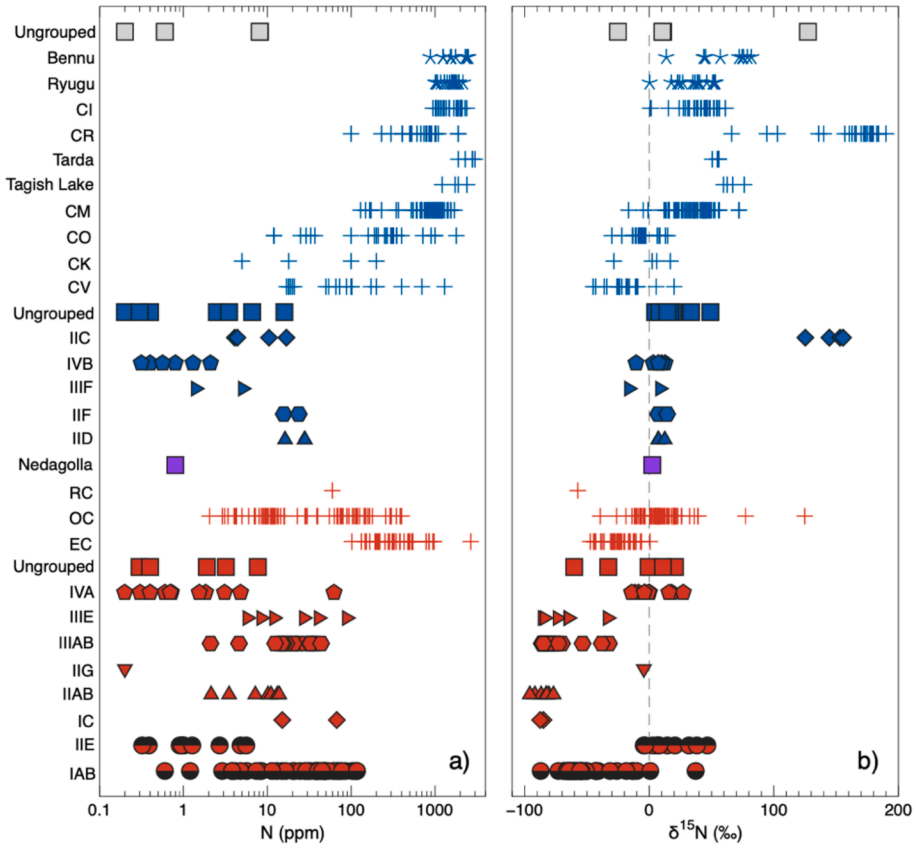

Fig. 1. a) Abundance and b) isotopic composition of N released by stepped heating of alloy fragments from grouped and ungrouped iron meteorites, compared with chondrites and samples returned from the asteroids (162173) Ryugu and (101955) Bennu. Samples from the NC and CC reservoirs are shown in red and blue, respectively. The ungrouped iron Nedagolla (purple square) is the only iron meteorite with a Mo-Ru-Ni isotopic composition intermediate between the NC and CC reservoirs (Spitzer et al., 2022). Ungrouped irons of unknown heritage are represented by gray squares. Groups IIAB and IIG likely originate from the same planetesimal core (Wasson and Choe, 2009; Anand et al., 2024). Data sources: iron meteorites (Pepin and Becker, 1982; Franchi et al., 1993; Prombo and Clayton, 1993; Mathew et al., 2000; Sugiura et al., 2000; Ponganis and Marti, 2007; Murty et al., 2019; Gamblin et al., 2026); chondrites (Injerd and Kaplan, 1974; Kung and Clayton, 1978; Thiemens and Clayton, 1981, 1983; Robert and Epstein, 1982; Grady et al., 1983, 1986, 2002; Lewis et al., 1983; Kerridge, 1985; Sugiura and Zashu, 1993; Hashizume et al., 1995, 2024; Sugiura et al., 1998; Sephton et al., 2003; Pearson et al., 2006; Alexander et al., 2012, 2018, 2013; Füri et al., 2013; Chan et al., 2016; Vacher et al., 2020, 2025; Marrocchi et al., 2021; Laize-Générat et al., 2024; Patzek et al., 2025; Marrocchi et al., 2026); Ryugu (Nakamura et al., 2022; Naraoka et al., 2023; Oba et al., 2023; Gamblin et al., 2024; excluding the pellets of Okazaki et al., 2023; Broadley et al., 2023; Hashizume et al., 2024); Bennu (Lauretta et al., 2024; Barnes et al., 2025; Marty et al., 2025; Glavin et al., 2025). The dashed line at 0 ‰ in panel b) corresponds to the isotopic composition of atmospheric N_2 (Nier, 1950).

Nitrogen abundances of iron meteorites are highly variable, ranging from < 1 to > 100 ppm, as determined by chemical extraction (Nash and Baxter, 1947; Goel, 1970), neutron activation (Goel, 1970; Kothari and Goel, 1974; Shukla and Goel, 1981; Belai et al., 1995), and stepped heating or fusion analyses (Fig. 1**a**; Gibson and Moore, 1971, and references therein; Kothari and Goel, 1974; Pepin and Becker, 1982; Franchi et al., 1993; Prombo and Clayton, 1993; Mathew et al., 2000; Sugiura et al., 2000; Ponganis and Marti, 2007; Murty et al., 2019). At the core formation conditions recorded by iron meteorites (ΔIW = –3 to –1, where IW represents the oxygen fugacity, fO_2, reported in log units relative to the iron-wüstite buffer) (Grewal et al., 2024; Spitzer et al., 2025a), N behaves as a siderophile element ($D_N^{metal-silicate} = [N]_{metal}/[N]_{silicate} =$ 10 –100 for alloy melts containing < 0.8 wt% C; Grewal et al., 2021a). This implies that N preferentially partitioned into the segregating Fe-Ni alloy during core-mantle differentiation. During subsequent cooling and fractional crystallization of the metallic melt, N was distributed between trapped alloy melt, γ-Fe,Ni (taenite; face-centered cubic, austenitic iron), α-Fe,Ni (kamacite; body-centered cubic, ferritic iron), and, in some cases, exsolved into nitrides. This process was controlled by the concentrations of Ni and non-metals (including C, S, and P) in the alloy, the cooling rate, associated phase transformations, and diffusive redistribution (Wriedt and Gonzalez, 1961; Sugiura, 1998; Grewal and Asimow, 2023; Pathak and Dasgupta, 2024). In most iron meteorites, taenite is the primary N carrier, except when nitrides such as carlsbergite (CrN) or roaldite ($(Fe, Ni)_4N$) are present (Buchwald and Scott, 1971; Nielsen and Buchwald, 1981), whereas kamacite is N-poor (Sugiura, 1998; Sugiura et al., 2000). These findings align with observations in steel metallurgy, where N is more soluble in the face-centered cubic structure of taenite, with N atoms apparently occupying the octahedral lattice sites (Gibson and Moore, 1971, and references therein). Minor amounts of N have also been measured in troilite based on bulk analyses (1–22 ppm; Prombo and Clayton, 1993; Murty and Marti, 1994), and *in situ* measurements indicate the presence of N in graphite and carbide inclusions, although their concentrations could not be quantified (Sugiura, 1998). The observed intra- and inter-sample variations in N content among iron meteorites of a given group (Fig. 1**a**) can thus be attributed, in part, to the sampling of Fe-Ni phases with distinct N abundances—kamacite *versus* taenite—as well as to the heterogeneous distribution of nitrides and various inclusions or accessory phases (e.g., Murty et al., 1983; Prombo and Clayton, 1993). As a result, it is unclear which data best represent the 'average' bulk N concentration of a given sample or group. Consequently, N abundance measurements of small iron meteorite samples—obtained using various analytical techniques—can be challenging to interpret and may not be directly applicable to inferring the N content of their parent cores and bulk parent bodies.

Iron meteorite fragments show a remarkably wide range of $\delta^{15}N$ values, from –95.8 ‰ to +155.6 ‰ (Fig. 1**b**; Pepin and Becker, 1982; Franchi et al., 1993; Prombo and Clayton, 1993; Murty and Marti, 1994; Mathew et al., 2000; Sugiura et al., 2000; Ponganis and Marti, 2007; Murty et al., 2019; Gamblin et al., 2026). *In situ* analyses by secondary ion mass spectrometry (SIMS) demonstrated that the isotopic composition of N in taenite is comparable to that of bulk samples, whereas graphite, carbide, and nitride inclusions show more variable $\delta^{15}N$ values (Sugiura, 1998; Sugiura et al., 2000). The isotopic composition of N in kamacite has not been determined to date, largely because its N concentration is too low to permit isotopic analysis by SIMS (Sugiura, 1998). Although variations exist within and between samples (Fig. 1**b**), each group of magmatic iron meteorites appears to have a relatively well-defined average N isotopic composition (Grewal et al., 2021b), which, in most cases, is thought to reflect the isotopic signature of its parent body at the time of alloy-silicate separation. This inference is supported by high-pressure, high-temperature experiments and *ab initio* calculations, which indicate that neither core-mantle differentiation (Grewal et al., 2022a) nor fractional crystallization of alloy melt (Grewal et al., 2025) significantly affects N isotope ratios (although the magnitude and direction of N isotope fractionation between alloy and silicate melt remain debated; Li et al., 2016; Dalou et al., 2019; Shi et al., 2022). Additional support comes from the absence of a correlation between $\delta^{15}N$ values and Ni or Ir contents in IIAB and IIIAB irons (Prombo and Clayton, 1993). Secondary modifications are also not considered to have significantly altered N isotopic compositions. Incorporation of isotopically light N_2 from the protosolar nebula ($\delta^{15}N_{PSN} = -383 \pm 8$ ‰; Marty et al., 2011) during parent body accretion or subsequent disruption can be ruled out (Grewal et al., 2021b), as the partial pressure of N_2 in the nebular gas was too low for significant ingassing (≤0.1 ppm) into Fe-Ni alloys, a conclusion supported by thermodynamic equilibrium calculations (Fegley, 1983). Furthermore, solar noble gases have only been detected in the ungrouped iron meteorite Washington County (Hintenberger et al., 1967; Becker and Pepin, 1987; Vogt et al., 2021), suggesting that neither nebular gases nor solar-wind-derived gases carried by irradiated solids were efficiently incorporated into core-forming alloys. Cosmic ray-induced spallation effects on N isotopic ratios in irons are negligible in most cases, despite their prolonged cosmic ray exposure (CRE) histories in space (e.g., ~675 ± 100 Myr for IIIAB irons; Voshage and Feldmann, 1979). Since cosmogenic (or 'spallogenic') ^{15}N is primarily produced by reactions with oxygen (Reedy, 1981; Mathew and Murty, 1993), N isotopic ratios of metallic phases remain largely unaffected by spallation, although spallation effects of up to 30 ‰ have been reported in irons containing numerous silicate inclusions or in specimens particularly poor in N (Franchi et al., 1993; Mathew et al., 2000). Collectively, these observations imply that the N isotopic compositions of most iron meteorites reflect the characteristics of their respective bulk parent bodies at the time of differentiation and are primarily controlled by the nature of the accreted material, with minimal influence from solar gas or spallation. Based on the available dataset (Fig. 1**b**), Grewal et al. (2021) therefore concluded that the earliest planetesimals in the inner and outer protoplanetary disk accreted isotopically distinct N, as NC irons predominantly exhibit negative $\delta^{15}N$ values (≤–90 ‰), whereas CC irons are characterized by higher $\delta^{15}N$ values (up to +155.6 ‰) (see also Rubin, 2018). However, given that many NC and CC iron meteorites (and chondrites) have overlapping N isotopic compositions (Fig. 1**b**), the ultimate origin—and even the existence—of an NC-CC isotopic dichotomy for N is still debated. Moreover, it remains uncertain to what extent volatile loss during early (hydro)thermal planetary processing, prior to the onset of melting and differentiation, and impact-induced exposure of core material to space may have modified the original N isotopic composition of the iron meteorite parent bodies or core fragments.

To improve our understanding of the N isotope systematics of iron meteorites, and, ultimately, of N isotopic variations in the protoplanetary disk during the first few million years of its history, we report coupled N–Ne–Ar isotopic data for poorly studied iron meteorite groups (IIG, IID) as well as ungrouped irons of NC or CC heritage. These new measurements, obtained by CO_2 laser heating and multi-collection noble gas mass spectrometry, provide critical constraints on the presence of solar-derived gases and on the magnitude of cosmogenic ^{15}N contributions, based on Ne and Ar abundances and isotopic compositions. The N dataset is then used to evaluate whether the N isotopic compositions of iron meteorites reflect primary signatures inherited by their parent bodies at the time of accretion, secondary modifications from parent body processes or mantle stripping, or a combination of both. Finally, the results are interpreted in the context of early N isotopic heterogeneity within the protoplanetary disk. Specifically, we explore how evolving condensation and evaporation fronts may have influenced the distribution of isotopically distinct N-bearing phases (including nitrides, organics, and ammonia ice) within the accretion regions of differentiated and undifferentiated planetesimals in the inner and outer disk.

2. Samples and analytical methods

2.1. Iron meteorite samples

A total of 28 iron meteorites were analyzed in this study (Table 1). These include 14 grouped irons from the IIAB (Ainsworth, Braunau, Coahuila, Guadalupe y Calvo, Mount Joy, North Chile, Sikhote Alin), IIG (Bellsbank, Guanaco, La Primitiva, Tombigbee River, Twannberg), and IID groups (Carbo, Rodeo), as well as 14 ungrouped irons (ALHA 77255, Babb's Mill, EET 83230, Grand Rapids, Guffey, Guin, Hammond, ILD 83500, La Caille, New Baltimore, NWA 859, NWA 6932, Santiago Papasquiero, Tishomingo).

Table 1
Iron meteorites analyzed in this study.

Sample	Source	Item No.	Ni* (wt. %)	Ge* (μg/g)	$(Ge/Ni)_{CI}$*
IIAB group, NC iron meteorites					
Ainsworth	Field Museum Chicago	ME 977	5.9	142	0.78
Braunau	NHM Vienna		5.1	185	1.18
Coahuila	MNHN Paris	2974	5.5	181	1.08
Guadalupe y Calvo	University of Münster		5.1	178	1.14
Mount Joy	JNMC Zürich		5.7	183	1.10
North Chile	University of Münster		5.6	185	1.07
Sikhote Alin	JNMC Zürich		5.9	160	0.93
IIG group, NC iron meteorites					
Bellsbank	NHM London	BM. 1961,403. UNG RH	4.4	54	0.40
Guanaco	Smithsonian Institution	USNM 7198	4.4	71	0.52
La Primitiva	NHM London	BM. 1927,77 UNG	4.8	38	0.26
Tombigbee River	NHM London	BM. 84646	4.2	62	0.48
Twannberg	Naturhist. Museum Bern	NMBE 43620, mass TW185	4.4	51	0.38
IID group, CC iron meteorites					
Carbo	University of Münster		10.1	88	0.28
Rodeo	University of Münster		10.3	93	0.29
Ungrouped, NC iron meteorites					
EET 83230	University of Münster		15.7	0.07	0.0001
Guin (non-magmatic)	University of Münster		9.2	144	0.50
NWA 859 (non-magmatic)	University of Münster		17.3	2123	3.98
Santiago Papasquiero	Smithsonian Institution	USNM 2603	7.5	0.04	0.0001
Ungrouped, CC iron meteorites					
ALHA 77255	University of Münster		12.3	0.06	0.0001
Babb's Mill (Troost's iron)	NHM London	BM. 18490	17.7	41	0.075
Grand Rapids	NHM London	BM. 68724	9.2	14	0.049
Guffey	Smithsonian Institution	USNM 4832	9.7	0.11	0.0003
Hammond	Smithsonian Institution	USNM 471	8.2	58	0.23
ILD 83500	University of Münster		17.5	48	0.089
La Caille	Field Museum Chicago	ME 902 #2	9.3	21	0.075
New Baltimore	Smithsonian Institution	USNM 710	6.5	37	0.19
NWA 6932	Smithsonian Institution	USNM 7612	12.3	102	0.27
Tishomingo	Smithsonian Institution	USNM 5862	32.4	0.09	0.0001

*Data were downloaded from Astromat Synthesis (https://astromat.org/) on June 5, 2025, using the following parameters: Sample = Meteorite name; Chemical variables = Trace Element: (Ge, Ni).

The IIAB and IIG groups both belong to the NC reservoir (Kruijer et al., 2017; Anand et al., 2024). Group IIAB is one of the largest magmatic iron meteorite groups, with over 150 known members, whereas group IIG is much smaller, consisting of only six identified samples. IIAB and IIG irons have low Ni contents (5.3–6.9 wt% and 4.2–4.9 wt%, respectively) (Fig. 2; Table 1); while all IIG irons and the low Ni (<5.75 wt%) members of the IIAB group are so-called hexahedrites that have a single crystal structure of kamacite, the higher Ni (5.75–6.9 wt%) members of group IIAB display a Widmanstätten pattern with kamacite widths of 5–10 mm and are, thus, referred to as coarsest octahedrites (Yang and Goldstein, 2005; Wasson and Choe, 2009). IIAB irons have the highest S contents of any magmatic iron meteorite group, consistent with their elevated concentrations of other volatile siderophiles, particularly Ga and Ge (Fig. 2; Wasson et al., 2007). In contrast, IIG irons are exceptionally S-poor and P-rich (Wasson and Choe, 2009). Despite these chemical differences, both groups are inferred to have formed from immiscible liquids within the same planetesimal core. Fractional crystallization models indicate that the IIAB core contained significant amounts of S and P (Chabot, 2004; Zhang et al., 2024). During the final stages of core solidification, a buoyant, S-rich liquid likely separated, leaving behind a S-poor, P-enriched residue (Wasson

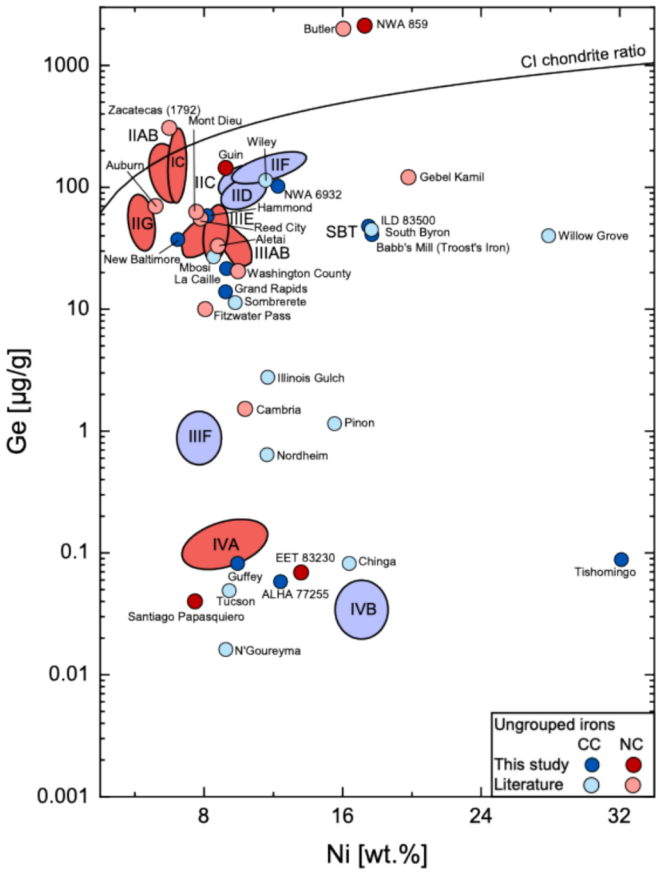

Fig. 2. Ge *versus* Ni contents of iron meteorites, including the compositional fields of the magmatic iron meteorite groups (Scott and Wasson, 1975). The 14 ungrouped irons analyzed in this study are shown in dark colors. The CI chondrite ratio is from Anders and Grevesse (1989). Data for the ungrouped irons are from the Astromaterials Data System (Astromat Synthesis) and Spitzer et al. (2025a).

et al., 2007). Wasson and Choe (2009) proposed that the IIG group samples this late-stage residual melt from the IIAB core. Combined Fe-Ni-O-Cr isotope data for IIAB and IIG irons recently confirmed a strong genetic link between the two groups, reinforcing the conclusion that both groups originate from the same core (Anand et al., 2024).

The IID irons, which originate from a CC-type parent body (Kruijer et al., 2017), contain 9.8–11.3 wt% Ni (Fig. 2; Table 1) and are structurally classified as fine to medium octahedrites. Their high Ga and Ge abundances indicate a volatile-rich precursor material. Despite their volatile-rich nature, this group is notably S-depleted, likely as a result of the early formation and extraction of a S-rich melt from the core as opposed to loss by devolatilization (Wasson and Huber, 2006; Zhang et al., 2024).

Ungrouped iron meteorites have chemical compositions that cannot be associated with any of the recognized groups through fractional crystallization models. Since each ungrouped iron meteorite may originate from a distinct parent body, they are highly valuable for studying a diverse range of early-accreted planetesimals. Recent Mo isotope measurements by Spitzer et al. (2025a) have provided genetic information for the ungrouped irons analyzed in this study, allowing for the determination of their origins within either the NC (EET 83230, Guin, NWA 859, Santiago Papasquiero) or CC reservoir (ALHA 77255, Babb's Mill, Grand Rapids, Guffey, Hammond, ILD 83500, La Caille, New Baltimore, NWA 6932, Tishomingo) (Fig. 2; Table 1). Notably, all of these are magmatic irons, except for Guin and possibly NWA 859. Guin's Ir/Au ratio of 4.3 falls within the typical range observed for non-magmatic irons (Spitzer et al., 2025a), and the presence of silicate inclusions is a key feature commonly associated with this type (Rubin et al., 1986). In contrast, NWA 859 has a notably low Ir/Au ratio (<1), a value typically indicative of a magmatic origin, and no silicate inclusions have been identified in this meteorite. Its young Hf-W model age, however, suggests a late-stage metal-silicate fractionation event (or multiple events), inconsistent with the formation history of magmatic irons. This led Spitzer et al. (2025a) to propose that NWA 859 is of non-magmatic origin. Notably, the chemical similarity of NWA 859 and Butler—particularly their extremely high Ge contents (Fig. 2)—suggests they originate from a common parent body (Wasson, 2011); the Ge isotopic composition and the Ga/Ni ratio of Butler are consistent with non-magmatic iron values (Luais, 2012).

2.2. Noble gas (Ne, Ar) and N extraction

At the noble gas facility of the Centre de Recherches Pétrographiques et Géochimiques (CRPG, Nancy, France), noble gases (Ne and Ar) and N were extracted from the iron meteorite samples under static vacuum by laser heating. Alloy fragments (3.4 to 14.2 mg) were placed into separate pits within a ZnSe-windowed laser chamber. The chamber was then connected to the gas purification line of the Noblesse–HR noble gas mass spectrometer, pumped to ultra-high vacuum (~10^{-9} Torr), and baked at ~ 100 °C overnight to remove adsorbed atmospheric gases from both the inner surfaces of the laser chamber and the sample surfaces. The iron meteorite fragments were heated with a 10.6 μm-wavelength CO_2 laser operated in continuous mode, with positioning controlled by a motorized x-y-z stage and real-time monitoring via a CCD camera positioned above the extraction chamber. The IIAB, IID, and ungrouped irons were heated in 2–4 steps at increasing relative power up to near maximum using a 30 W Melles Griot™ laser (Humbert et al., 2000) during an analytical campaign spanning several months, for which absolute laser power was not controlled. The IIG irons were analyzed during a separate campaign using a 32 W MIR10^2 laser (Elemental Scientific) at 20 % (step 1) and 100 % (steps 2 and 3) of maximum power.

Limitations of this method are that Fe-Ni alloy fragments cannot be fully melted, potentially affecting the efficiency of noble gas and N extraction, and that the temperature achieved during laser heating cannot be measured. Additionally, repeated heating at high temperatures led to the accumulation of metal vapor deposits on the laser chamber window. This reduced the heating efficiency and visibility of some samples, and, in at least one case (e.g., heating step 4 of North Chile), increased laser beam absorption and caused slight heating of the ZnSe lens. Reflection of the laser beam from the metallic sample surface may also have contributed to variable contamination through secondary heating of the chamber walls or window, the magnitude of which may differ between individual heating steps and different samples. Despite these methodological limitations, previous application of this analytical approach to IIIAB iron meteorites yielded N abundances and isotopic compositions consistent with literature data (Gamblin et al., 2026), demonstrating that the method provides reliable N systematics for meteorite metal.

2.3. Noble gas (Ne, Ar) and N purification and static mass spectrometry analysis

The extracted gas fraction was split into two calibrated volumes for specific purification of noble gases and N (see the detailed procedures in Zimmermann and Füri, 2015; Zimmermann et al., 2015). Noble gases were purified in an all-metal purification line using a hot (600 °C) Ti sponge getter and two cold (room temperature) SAES™ Ti-Al getters. Argon was separated from Ne by adsorption onto a charcoal finger held at –196 °C with liquid N_2. In parallel, N was purified within a Pyrex and quartz-glass line. Nitrogen (along with other species such as H, C, S) was oxidized by the O_2 released from CuO sticks heated from 450 °C to 900 °C over 25 min. Oxidized species were trapped in a U-shaped cold trap at –180 °C, except NO_X. The CuO sticks were then gradually cooled in 100 °C intervals down to 300 °C (15 min per step) to re-absorb excess O_2 and reduce NO_X to molecular N_2. A second cold trap, consisting of a glass finger with platinum foils, held at –175 °C, was used from 600 °C onwards to enhance trapping of impurities such as H_2O, CO_2, and C_xH_y. Before introducing the purified gas into the mass spectrometer, an ion gauge was used to control the pressure, and, if necessary, the N_2 amount was adjusted by volume dilution to match the pressure of air standards, which were purified using the same procedure.

Ne–Ar–N_2 abundances and isotope ratios were measured sequentially using a 3F4M Noblesse–HR (Nu Instruments) multi-collector noble gas mass spectrometer at a trap current of 150 μA (Zimmermann et al., 2025). Source (i.e., extraction and ion repeller voltages) and zoom optics settings were optimized for each gas to maximize sensitivity and minimize instrumental mass fractionation, and to achieve high mass resolution (~700) and mass resolving power (~7000), respectively. The three Ne isotopes were measured simultaneously over 25 cycles on three ion counters ($^{22}Ne^+$ on IC0, $^{21}Ne^+$ on IC2, $^{20}Ne^+$ on IC3). Throughout the analytical sequence, a charcoal finger held at –196 °C and two GP-50 SAES getters, connected to the source and detector blocks, minimized contributions from $^{40}Ar^{2+}$ and $^{44}CO_2^{2+}$ to the $^{20}Ne^+$ and $^{22}Ne^+$ signals, respectively. The $^{40}Ar^{2+}$ signal was monitored but no correction was applied to the $^{20}Ne^+$ signal due to partial peak separation. The $^{22}Ne^+$ signal was corrected for $^{44}CO_2^{2+}$ using a measured $^{44}CO_2^{2+}/^{44}CO_2^+$ ionization ratio of 0.55 %, though the interference (1–4 cps) was negligible relative to the total $^{22}Ne^+$ counts. The $^{21}Ne^+$ signal was measured at the peak center without $^{20}NeH^+$ correction given the low hydrogen background maintained by the getters. After Ar was released from the charcoal finger and purified, the three Ar isotopes were analyzed in multi-collection mode over 25 cycles ($^{40}Ar^+$ on Fa0 [10^{11} Ω], $^{38}Ar^+$ on IC2, $^{36}Ar^+$ on IC3). The N_2 isotopologues were also analyzed in multi-collection mode for 25 cycles ($^{14}N^{14}N^+$ on Fa2 [10^{11} Ω], $^{14}N^{15}N^+$ on Fa1 [10^{12} Ω], and $^{15}N^{15}N^+$ on IC0), with $^{12}C^{16}O^+$ monitored on Fa2 to correct N_2 signals for CO. Following data acquisition, the $^{12}C^{16}O^+$ signal was directly subtracted from $^{14}N^{14}N^+$, whereas contributions of $^{13}C^{16}O^+$ and $^{12}C^{18}O^+$ to the $^{14}N^{15}N^+$ and $^{15}N^{15}N^+$ signals, respectively, were estimated from natural $^{12,13}C$ and $^{16,18}O$ abundances.

Sensitivity and instrumental mass fractionation were monitored through repeated analyses of purified air standard aliquots during the two measurement periods. Procedural blanks (with the laser off) were

measured prior to the sample analyses and averaged $3.2 \pm 0.6 \times 10^{-16}$ mol ^{20}Ne, $2.9 \pm 1.4 \times 10^{-17}$ mol ^{36}Ar, and $4.2 \pm 1.3 \times 10^{-12}$ mol N_2 for the first analytical campaign, and $2.3 \pm 0.1 \times 10^{-16}$ mol ^{20}Ne, $3.2 \pm 0.9 \times 10^{-17}$ mol ^{36}Ar, and $4.9 \pm 1.6 \times 10^{-12}$ mol N_2 for the second campaign. Consequently, N_2 blank contributions—with near-atmospheric isotopic compositions—amounted to $\geq$ 10 % for the highest-power steps of Guadalupe y Calvo and Braunau (IIAB), Tombigbee River, Bellsbank, and La Primitiva (IIG), as well as Santiago Papasquiero, whereas all other analyzed irons released larger N amounts. Extracted Ne–Ar–N_2 abundances (in mol) and corresponding isotope ratios were corrected for blanks, sensitivity, and instrumental mass fractionation. Nitrogen isotope ratios are reported in delta notation, calculated for N_2 as $\delta^{15}N$ (‰) = $\{[1 + 2 \times (^{28}N_2/^{29}N_2)_{atm}] / [1 + 2 \times (^{28}N_2/^{29}N_2)_{measured}] - 1\} \times 1000$, where $(^{28}N_2/^{29}N_2)_{atm}$ is the isotopic composition of atmospheric N_2 (136.05; Nier, 1950). Reported uncertainties (1σ s.d.) for $\delta^{15}N$ values reflect the reproducibility (s.d.) of purified air standard measurements (0.5 ‰ and 1 ‰ for the two analytical sessions), with negligible contribution from analytical precision. Blank-corrected abundances and isotope ratios of Ne–Ar–N extracted at different laser heating steps from each of the 28 iron meteorites are reported in Supplementary Table S1. Heating steps for which the blank contribution to the measured noble gas abundances represents $\geq$ 30 % are not reported.

3. Results

3.1. Noble gas (Ne, Ar) isotope ratios

Small amounts of noble gases (Ne, Ar) were released from the iron meteorite fragments at most heating steps. The measured ^{20}Ne/^{22}Ne, ^{21}Ne/^{22}Ne, and ^{36}Ar/^{38}Ar ratios indicate that the noble gases are of cosmogenic origin (Fig. 3), implying they were produced by spallation reactions during exposure of the iron meteoroids to galactic cosmic rays in space. In addition, an atmospheric noble gas component was detected during the heating of several samples, possibly adsorbed onto the sample or laser chamber surfaces and not fully removed during bakeout. In the case of North Chile, atmospheric noble gases were also measured during the fourth high-temperature heating step. However, at this stage, vapor deposits from previous steps had coated the interior surface of the laser chamber window, causing the ZnSe lens to become opaque and absorptive; this may have resulted in partial heating of the lens itself by the laser beam. No traces of noble gases from the solar nebula or solar wind were detected in any of the iron meteorites.

3.2. Spallation effects on N isotope ratios

Cosmogenic ^{15}N is produced from oxygen atoms (^{16}O) by cosmic ray-induced spallation reactions at a rate that depends on both a meteoroid's size and the depth of a given sample within the irradiated body (Reedy, 1981; Mathew and Murty, 1993). While $^{15}N_{cosm}$ production in silicates can be substantial (e.g., Füri et al., 2015; Gamblin et al., 2026), its contribution in Fe-Ni alloys has been considered negligible in most previous studies of N in iron meteorites (Franchi et al., 1993; Prombo and Clayton, 1993; Murty and Marti, 1994; Sugiura et al., 2000; Ponganis and Marti, 2007). Only Mathew et al. (2000) argued for a significant correction—up to –30 ‰ for two samples—to the $\delta^{15}N$ values measured in N-poor IVA irons and in silicate inclusion-rich IIE irons. In most cases, however, their proposed corrections were much smaller, on the order of a few per mil. Their conclusions were based on coupled noble gas (He, Ne, Ar)–N analyses and the assumption of a constant, shielding-independent $(^{21}Ne/^{15}N)_{cosm}$ production rate ratio of 0.80. Notably, the underlying noble gas abundances and isotope ratios were not published, and spallation corrections for N-poor IVB irons analyzed in the same study could not be applied because corresponding noble gas data were missing. In addition, unlike all other studies, Mathew et al. (2000) considered only N released at temperature steps $\geq$ 1050 °C as 'trapped' or 'indigenous', excluding N released below this threshold on the assumption that it reflected contamination or originated from nonmetallic phases. This methodological difference complicates direct comparisons of their spallation-corrected $\delta^{15}N$ values with other datasets.

Although total $^{21}Ne_{cosm}$ abundances for the iron meteorite fragments analyzed in this study may be slightly underestimated (see **Section 2.2.**), such that corresponding CRE ages were not derived, a $^{15}N_{cosm}$ correction can still be applied at each heating step based on the amount of extracted $^{21}Ne_{cosm}$ and the $(^{21}Ne/^{15}N)_{cosm}$ production rate ratio of Mathew et al. (2000). In this case, the magnitude of the correction is smaller than the uncertainty associated with each measured $\delta^{15}N$ value (i.e., <1 ‰), rendering the correction insignificant. Consequently, only the measured $\delta^{15}N$ values—without any correction for $^{15}N_{cosm}$—are considered in the following discussion. These values are also more directly comparable to the N isotopic data of iron meteorites reported in the literature.

3.3. Nitrogen isotope ratios

The 'bulk' N concentrations estimated here, corresponding to summed N amounts extracted by laser heating and normalized to sample

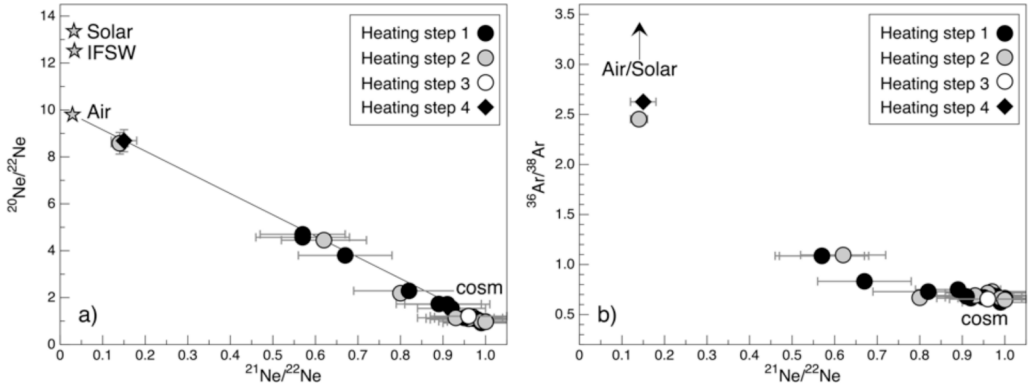

Fig. 3. a) ^{20}Ne/^{22}Ne *versus* ^{21}Ne/^{22}Ne and b) ^{36}Ar/^{38}Ar *versus* ^{21}Ne/^{22}Ne for noble gases extracted from iron meteorite fragments at different heating steps. The isotopic signatures of the Sun's outer convective zone (Solar; ^{20}Ne/^{22}Ne = 13.36 and ^{21}Ne/^{22}Ne = 0.03226; Heber et al., 2009; Ott, 2014), implantation-fractionated solar wind (IFSW, previously called Ne-B; Black, 1972), and the terrestrial atmosphere (Air; ^{20}Ne/^{22}Ne = 9.80 and ^{21}Ne/^{22}Ne = 0.0288–0.0290; Eberhardt et al., 1965; Györe et al., 2019; Wielandt and Storey, 2019; Saxton, 2020) are shown for comparison. The solid line in a) represents a mixing line between the cosmogenic component (cosm; ^{20}Ne/^{22}Ne ≈ ^{21}Ne/^{22}Ne ≈ 1) and atmospheric Ne. Most measured Ne isotope ratios have large uncertainties (1σ s.d.) due to the small amounts of gas released.

mass, for the IIAB irons (4.7–19.3 ppm N; excluding Guadalupe y Calvo and Braunau with low N yields of 0.4 and 1.9 ppm N, respectively), IIG irons (0.1–2.3 ppm N), and IID irons (13.7–32.3 ppm N) overlap with previously reported ranges for the same groups (2.1–13.9, 0.2, and 16.3–27.8 ppm N, respectively; Prombo and Clayton, 1993; Franchi et al., 1993; Murty et al., 2019). This agreement suggests that any effects of non-quantitative N extraction associated with the absence of melting did not substantially affect the estimated N concentrations, and by extension the derived isotopic compositions, for almost all samples considered. The N isotopic compositions of IIAB, IIG, IID, and ungrouped iron meteorites determined in this study (see Supplementary Table S1) are shown in Fig. 4, together with literature data (see compiled data at https://doi.org/10.24396/ORDAR-185). The $\delta^{15}N$ values from this study represent abundance-weighted averages derived from 2 to 4 laser heating steps per sample, whereas the literature values correspond to summed N isotopic compositions obtained from two combustion steps at 1160 °C (sample sizes of ~ 7 to 50 mg; Pepin and Becker, 1982), repeated combustion at 1250 °C (1.4 to 12.9 mg; Franchi et al., 1993), or pyrolysis at temperatures up to 1800 °C (~5 g; Prombo and Clayton, 1993) and 1700 °C (180 mg; Murty et al., 2019).

In this study, the three IIAB octahedrites Ainsworth, Sikhote-Alin, and Mount Joy were found to have low $\delta^{15}N$ values ranging from –92.0 ‰ to –83.6 ‰. The IIAB hexahedrite North Chile yielded comparable $\delta^{15}N$ values of –94.5 ‰ to –84.9 ‰ across four heating steps, resulting in an abundance-weighted average of –93.3 ‰, while Coahuila recorded a $\delta^{15}N$ value of –82.9 ‰ based on two steps. Previous pyrolysis or combustion analyses produced similar $\delta^{15}N$ values for Sikhote-Alin (–82.2 ‰; Prombo and Clayton, 1993), Coahuila (–91.8 ‰ and –86.7 ‰; Prombo and Clayton, 1993) and four other IIAB iron meteorites (–95.8 ‰ to –76.8 ‰ in Uwet, Navajo, Hex River Mountains, and Raghunathpura; Franchi et al., 1993; Prombo and Clayton, 1993; Murty et al., 2019). Roaldite in Sikhote-Alin also yielded a comparable $\delta^{15}N$ value of –90.7 ‰, as determined by SIMS (Sugiura, 1998). In contrast, the two IIAB hexahedrites Guadalupe y Calvo and Braunau showed distinct N isotope ratios ($\delta^{15}N \approx$ –5.6 ‰ to –0.5 ‰), much closer to the isotopic composition of atmospheric N_2, but released only small amounts of N during laser heating compared to the other IIAB irons. Notably, Guadalupe y Calvo and Braunau are the two most Ni-poor IIAB members analyzed in this study (Table 1) and are therefore not expected to contain taenite. Because taenite is the primary N-bearing phase in iron meteorites (Sugiura, 1998; Sugiura et al., 2000), taenite-poor samples are expected to retain less indigenous N and to be more susceptible to contamination effects, consistent with their elevated apparent $\delta^{15}N$ values.

A similar pattern was observed for the IIG group. Twannberg and Guanaco, which released N significantly above blank levels (~2.3 ppm), yielded $\delta^{15}N$ values of –104.8 ‰ and –94.4 ‰, respectively, whereas Tombigbee River, Bellsbank, and La Primitiva released smaller N amounts (<0.2 ppm) with higher $\delta^{15}N$ values (–27.5 ‰ to –9.8 ‰), much closer to the isotopic composition of atmospheric N_2. Notably, the only previously published $\delta^{15}N$ value for a IIG iron meteorite (Tombigbee River) was –4.3 ‰, but this sample was also N-poor (0.2 ppm; Prombo and Clayton, 1993) (Fig. 1). Since all IIAB and IIG irons are thought to originate from a common planetesimal core (Wasson and Choe, 2009; Anand et al., 2024), and N isotopic fractionation during core crystallization is minimal (≤1.2 ‰; Grewal et al., 2025), they are expected to record identical N isotopic compositions. On this basis, the highly elevated $\delta^{15}N$ values observed for five particularly N-poor hexahedrites—Guadalupe y Calvo, Braunau, Tombigbee River, Bellsbank, and La Primitiva—are most plausibly attributed to analytical artifacts. Extracting measurable amounts of N from small, N-poor kamacite fragments is inherently challenging, and minor contamination from residual atmospheric N_2, adsorbed onto sample surfaces or the interior of the laser chamber, can disproportionately affect the measured signal. Accordingly, these elevated $\delta^{15}N$ values are excluded from further discussion, and N in both the IIAB and IIG groups, as well as in

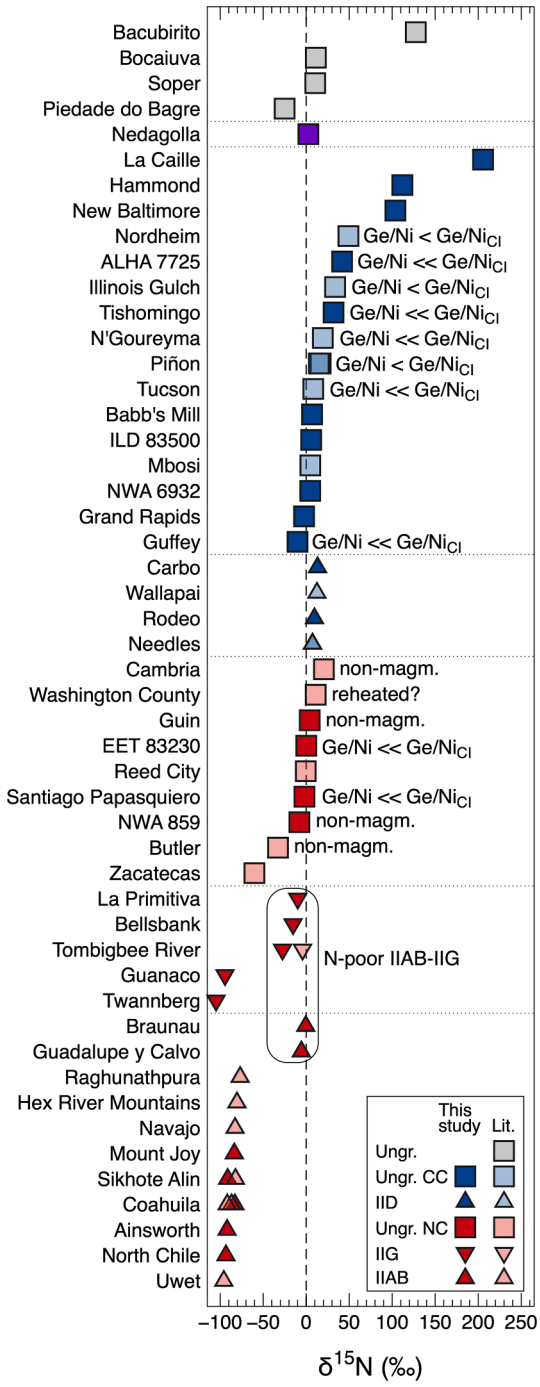

Fig. 4. Isotopic composition of N extracted from fragments of IIAB, IIG, IID, and ungrouped iron meteorites (summed over 2–4 individual laser heating steps; this study), compared to literature data (Pepin and Becker, 1982; Franchi et al., 1993; Prombo and Clayton, 1993; Murty et al., 2019; https://doi.org/10.24396/ORDAR-185). NC and CC irons are shown in red and blue, respectively, whereas ungrouped irons of unknown heritage are represented by gray squares. The ungrouped iron Nedagolla (purple square) is the only iron meteorite with a Mo-Ru-Ni isotopic composition intermediate between the NC and CC reservoirs (Spitzer et al., 2022). Groups IIAB and IIG are thought to originate from the same planetesimal core (Wasson and Choe, 2009; Anand et al., 2024). The $\delta^{15}N$ values of several irons may not directly reflect primary parent core isotopic compositions, either due to analytical artifacts (for N-poor IIAB and IIG hexahedrites) or because the iron meteorites are of non-magmatic origin or strongly volatile-depleted (i.e., with low Ge/Ni ratios; see **Fig. 2** and **Table 1**).

their common parent core, is inferred to be isotopically light. This N isotopic composition is best represented by the most N-rich samples—North Chile and Sikhote-Alin from this study, Sikhote-Alin from Prombo and Clayton (1993), and Uwet from Franchi et al. (1993)—which define an overall average $\delta^{15}N$ value close to –90 ‰.

The two IID medium octahedrites, Rodeo and Carbo, yielded $\delta^{15}N$ values of +9.6 ‰ and +13.2 ‰, respectively. Previously reported $\delta^{15}N$ values of +7.2 to +12.5 ‰ for two other IID irons (Needles, Wallapai) fall very close to this range (Franchi et al., 1993; Prombo and Clayton, 1993). Notably, all of these samples released significantly more N (13.7–32.3 ppm) than the particularly N-poor IIAB-IIG hexahedrites, demonstrating that the measured N isotope ratios are unaffected by atmospheric contamination. Although only four IID iron meteorites have been analyzed to date, the consistency of values across three independent studies indicates that the IID core is significantly enriched in ^{15}N compared to that of the IIAB and IIG groups.

The four NC ungrouped irons studied here released small amounts of N (0.1–4.4 ppm), comparable to N abundances reported for different NC ungrouped irons in the literature (0.3–7.7 ppm; Pepin and Becker, 1982; Prombo and Clayton, 1993). NWA 859 and Guin, which have been interpreted as non-magmatic (Spitzer et al., 2025a), showed $\delta^{15}N$ values of –7.9 ‰ and +4.1 ‰, respectively. The magmatic irons Santiago Papasquiero and EET 83230 recorded similar $\delta^{15}N$ values of –2.0 ‰ and +9.1 ‰, but both have low Ge/Ni and Ga/Ni ratios (Fig. 2; Table 1; Spitzer et al., 2025a), which may reflect loss of volatile elements from their parent cores (see **Section 4.1.** for details). In addition, Santiago Papasquiero, classified as a hexahedrite in the Meteoritical Bulletin Database, released the smallest amount of N during laser heating, rendering its isotopic measurement of limited reliability. Previous studies reported N isotopic compositions for five NC ungrouped irons (Pepin and Becker, 1982; Prombo and Clayton, 1993), including the non-magmatic irons Butler (–32.8 ‰) and Cambria (+20.6 ‰), the former of which may be co-genetic with NWA 859, as well as Washington County (+11.0 ‰), which experienced severe shock-induced reheating (Buchwald, 1975). Zacatecas (1792) and Reed City, presumed to be of magmatic origin (Spitzer et al., 2025a), were found to have $\delta^{15}N$ values of –60.2 ‰ and –0.5 ‰, with corresponding N abundances of 7.7 and 0.4 ppm, respectively. These literature data suggest that at least one planetesimal core from the NC reservoir was enriched in ^{15}N compared to those of the IC, IIAB–IIG, IIIAB, and IIIE groups (Fig. 1b and Fig. 4); this conclusion, however, rests entirely on the Reed City iron meteorite (Preston, 1903), which released only a very small amount of N (Prombo and Clayton, 1993).

The CC ungrouped irons Guffey, Tishomingo, and ALHA 77255, which are all characterized by low Ge/Ni ratios and relatively low N contents of 0.8 to 6.9 ppm (Table 1), showed $\delta^{15}N$ values between –10.1 ‰ and +41.7 ‰. The remaining ungrouped irons of CC origin—Grand Rapids (3.6 ppm N), NWA 6932 (34.6 ppm N), ILD 83500 (5.7 ppm N), Babb's Mill (6.0 ppm N), New Baltimore (49.3 ppm N), Hammond (19.5 ppm N), and La Caille (13.2 ppm N)—recorded $\delta^{15}N$ values ranging from –2.5 ‰ to +205.6 ‰. Previously, six CC ungrouped irons of magmatic origin were reported to have $\delta^{15}N$ values ranging from +4.8 ‰ to +49.1 ‰ (Pepin and Becker, 1982; Prombo and Clayton, 1993); however, Tucson and N'Goureyma have markedly low Ge/Ni ratios, whereas Piñon, Illinois Gulch, and Nordheim have intermediate Ge/Ni ratios comparable to those of the IIIF group (Fig. 2). Mbosi, with a $\delta^{15}N$ value of +4.8 ‰, appears undepleted in Ge and is N-rich (16.0 ppm). Overall, the $\delta^{15}N$ values of CC ungrouped iron meteorites extend to significantly higher levels than those of NC origin, reaching up to +205.6 ‰ in La Caille, and even exceeding the highest values observed in the IIC group (Fig. 1**b**). The lightest $\delta^{15}N$ values of CC irons, however, overlap with those of the NC ungrouped iron Reed City (–0.5 ‰). Thus, when all ungrouped irons of magmatic origin are considered, the measured N isotopic compositions do not show a clear NC-CC dichotomy; the significance of individual data points is discussed below.

4. Discussion

Previous studies of the N isotopic composition of iron meteorites have used variable analytical approaches, particularly in terms of sample sizes and extraction temperatures (see **Section 3.3.**). This methodological variability—including the small sample sizes analyzed by laser heating in the present study—has contributed to small discrepancies in the reported $\delta^{15}N$ values for individual iron meteorites or groups (Fig. 1**b** and Fig. 4). Despite these differences, a consistent overall pattern emerges across datasets. Non-carbonaceous irons from groups IC, IIAB–IIG, IIIAB, and IIIE contain isotopically light N. In contrast, IVA and NC-type ungrouped iron meteorites have higher $\delta^{15}N$ values, similar to those of CC-type irons from groups IID, IIF, IIIF, and IVB, and several CC-type ungrouped iron meteorites. Group IIC and three CC-type magmatic ungrouped irons show particularly elevated $\delta^{15}N$ values. These patterns raise key questions about what the N isotopic compositions of these samples truly reflect: primary signatures of their parent planetesimals at the time of accretion, secondary modifications due to parent body processes, or a combination of both. Disentangling primary, parent-body-specific source characteristics from secondary overprints is particularly challenging for N, given that it has only two stable isotopes. Consequently, additional chemical and petrological tracers or physicochemical parameters must be considered to develop a comprehensive understanding of N isotopic variations in meteoritic materials and their relationship to N isotopic heterogeneity and substructures in the early protoplanetary disk. Here, we address this challenge by first identifying the iron meteorites that most reliably preserve the primary N isotopic signatures of their parent bodies. This approach provides a framework for establishing accretionary relationships among differentiated and undifferentiated planetesimals. It also provides a basis for testing whether the distribution of isotopically distinct N-bearing phases (including nitrides, organics, ammonia ice), together with the condensation and evaporation fronts that controlled their incorporation into planetesimals across the protoplanetary disk, can account for the measured N isotopic variations in iron meteorites and chondrites.

4.1. Evidence for volatile loss in IVA, IVB, and a subset of ungrouped iron meteorites

Although N abundances in iron meteorite fragments are difficult to interpret (see **Section 1**), it is striking that members of both the magmatic IVA and IVB groups exhibit depletions in the major volatiles N (Fig. 1**a**) and C (Moore et al., 1969; Lewis and Moore, 1970; Goldstein et al., 2017), as well as in moderately volatile and siderophile elements such as Ga and Ge (Fig. 2; e.g., Scott, 1972; Scott and Wasson, 1975). These Ga and Ge depletions have been linked to a range of causes, including fractionation during nebular condensation prior to accretion (Kelly and Larimer, 1977; Sears, 1978; Campbell and Humayun, 2005; Corrigan et al., 2022), as well as various parent body processes (e.g., Rasmussen et al., 1984; Wasson et al., 2006; McCoy et al., 2011; Hirschmann et al., 2021). However, the highly variable metallographic cooling rates recorded by individual members of the IVA and IVB groups (Haack et al., 1996; Ruzicka and Hutson, 2006; Yang et al., 2007, 2008, 2011) imply that these iron meteorites originate from metal bodies that did not cool isothermally within mantle-insulated cores. Instead, the parent bodies of both groups are thought to have experienced grazing hit-and-run impacts (Asphaug, 2010), which stripped away their insulating mantles and exposed hot—possibly partially molten—core material. This scenario would have facilitated relatively rapid cooling, as well as volatilization and loss of Ga, Ge (e.g., Yang et al., 2007, 2008), and also Ag (Horan et al., 2012; Matthes et al., 2018). The low Ga/Ni and Ge/Ni ratios of the IVA and IVB groups are, therefore, currently best explained by volatile loss from iron cores following collisional disruption of their parent bodies.

Mantle removal and the associated pressure release from such disruptive collisions may also have led to evaporative N loss from

exposed solid or partially molten IVA and IVB core material, accompanied by isotopic fractionation. However, the extent of N loss and the magnitude of the expected increase in $\delta^{15}N$ are difficult to estimate, as both would have depended on multiple physicochemical parameters (e.g., vapor pressure, temperature, alloy composition, and potential recondensation reactions), and the resulting $\delta^{15}N$ values would also have been influenced by the mode of isotopic fractionation (equilibrium *vs*. kinetic). Consequently, the initial N inventories (Grewal and Asimow, 2023; Pathak and Dasgupta, 2024) and isotopic compositions of the IVA and IVB parent cores are challenging to reconstruct. Importantly, if substantial N loss and associated isotopic fractionation are responsible for the highly elevated $\delta^{15}N$ values observed in IVA irons relative to the other NC iron groups (Fig. 1**b**), and if similar processes affected the IVB core, this would imply that the IVB core originally had a negative $\delta^{15}N$ signature. This, in turn, would support an overlap in N isotopic compositions between NC– and CC-type irons.

The potential for impact-induced mantle stripping and associated evaporative volatile loss from planetesimal cores across the protoplanetary disk complicates efforts to constrain the primary N isotopic compositions of bodies sampled by ungrouped irons, several of which are also N-poor (Fig. 1**a**). While most ungrouped iron meteorites have Ga/Ni and Ge/Ni ratios closer to the chondritic value, a subset of five ungrouped magmatic iron meteorites in this study stands out for their very low Ge/Ni ratios similar to those of the IVA and IVB groups: the NC-type irons EET 83230 and Santiago Papasquiero, and the CC-type irons ALHA 77255, Guffey, and Tishomingo (Fig. 2; Table 1). Five CC-type magmatic irons previously analyzed by Pepin and Becker (1982) and Prombo and Clayton (1993) also show Ge depletion. Among these specimens, N'Goureyma and Tucson are as depleted as samples from the IVA and IVB groups, whereas Illinois Gulch, Nordheim, and Piñon show moderate depletions, comparable to the IIIF group (Fig. 2). The $\delta^{15}N$ values of these Ge-depleted specimens are not markedly different from those of their Ge-rich counterparts, but they also overlap with the $\delta^{15}N$ range of non-magmatic specimens (Fig. 1**b** and Fig. 4). Consequently, it remains uncertain whether their N isotopic compositions reflect primary signatures inherited during alloy-silicate separation or secondary modification by volatile loss.

4.2. N isotopic evidence for planetesimal formation sunward of the tar line

The NC magmatic iron meteorite groups IC, IIAB–IIG, IIIAB, and IIIE are characterized by low $\delta^{15}N$ values of –90 to –80 ‰ (based on results from this study, combined with abundance-weighted averages of bulk measurements of IC, IIIAB, and IIIE irons; Fig. 1**b** and Fig. 4). These isotopic signatures indicate that N in the mantle and core of four differentiated planetesimals—which accreted in the inner protoplanetary disk within the first ~ 1 Myr of Solar System history (Spitzer et al., 2021, Spitzer et al., 2025a)—was significantly less ^{15}N-depleted than the protosolar nebula gas ($\delta^{15}N_{PSN} = -383 \pm 8$ ‰; Marty et al., 2011), yet less ^{15}N-enriched than NC-type undifferentiated planetesimals sampled by Rumuruti chondrites ($\delta^{15}N_{RC} = -57.3$ ‰, based on PCA 91002; Sugiura and Zashu, 1993), enstatite chondrites ($\delta^{15}N_{EC} = -47.4$ to +0.6 ‰; Kung and Clayton, 1978; Grady et al., 1986), and unequilibrated ordinary chondrites ($\delta^{15}N_{UOC} = -39.2$ to +39.3 ‰; Kung and Clayton, 1978; Hashizume et al., 1995; Sugiura et al., 1998; Alexander et al., 2012; Vacher et al., 2025) (Fig. 1**b**). The ungrouped magmatic irons Zacatecas (1792) and Reed City, with $\delta^{15}N$ values of –60.2 ‰ and –0.5 ‰, respectively (Prombo and Clayton, 1993), may indicate that some NC iron meteorite parent bodies sampled isotopically heavier N than those represented by the grouped irons; however, at least with respect to the N-poor Reed City sample, this interpretation warrants further verification.

The observed differences in N isotopic composition among NC iron meteorites and chondrites—and, ultimately, among their differentiated and undifferentiated parent bodies—may provide important clues about the nature, evolution, and spatiotemporal distribution of N-bearing carrier phases in the inner protoplanetary disk. If all planetesimals—regardless of their accretion ages and formation zones in the inner or outer protoplanetary disk—accreted the same predominantly organic (and possibly presolar) N-bearing precursors, then the observed variability in N isotopic compositions among NC chondrites and iron meteorites may reflect N loss and an associated decrease in $\delta^{15}N$ during parent body processing (e.g., Alexander et al., 1998; Grewal, 2022). Nitrogen outgassing and any associated isotopic fractionation during large-scale melting were likely limited, because early-formed planetesimals, including the parent bodies of iron meteorites, are inferred to have developed internal magma oceans underneath insulating, possibly undifferentiated crusts (Grewal et al., 2022b; Zhang and Driscoll, 2025). However, ^{15}N loss could have occurred during early (hydro)thermal processing, prior to the onset of melting and differentiation. Both thermal metamorphism and aqueous alteration have been proposed to preferentially degrade and remove ^{15}N-rich organics from carbonaceous chondrite-type material, based on laboratory experiments (Alexander et al., 1998; Sephton et al., 2003) as well as correlations between the N abundance and isotope ratio with petrologic indicators of metamorphism or hydration (Pearson et al., 2006; Alexander et al., 2013). Thermal degradation experiments on bulk samples and isolated organics suggest that N-bearing compounds combust at $\leq$ 500 °C, with the most ^{15}N-enriched fractions released at even lower temperatures ($\leq$350–400 °C; Alexander et al., 1998; Sephton et al., 2003). In contrast, heating of insoluble organic matter (IOM) from the carbonaceous chondrite Orgueil resulted in no detectable N loss or change in bulk $\delta^{15}N$ (Remusat et al., 2019), highlighting both the uncertainty surrounding the efficiency of thermal N loss and the validity of the assumption that all planetesimals accreted common N-bearing precursors. In addition to these conflicting experimental findings, Grewal et al. (2025) observed that NC iron meteorites exhibit $\delta^{15}N$ values distinctly lower than those of chondrites that experienced the highest degrees of thermal metamorphism. This observation suggests that ^{15}N loss during early (hydro) thermal processing cannot fully account for the low $\delta^{15}N$ values in NC iron meteorites. Instead, these values likely reflect the accretion of isotopically distinct N-bearing precursors by iron meteorite parent bodies. In this scenario, thermal processing of ^{15}N-rich precursors may have occurred within the early protoplanetary disk itself, thereby influencing both the amount and isotopic composition of N available to planetesimals forming at different heliocentric distances and times (e.g., Bermingham et al., 2020; Broadley et al., 2022, and references therein).

The stability and distribution of N-bearing phases—primarily organics, along with reduced phases such as nitrides, carbides, graphite—in the inner protoplanetary disk were largely governed by physicochemical conditions, including the disk's thermal structure and oxygen fugacity. As temperature increased with decreasing heliocentric distance along the disk midplane, Lodders (2004) proposed that organics, including their refractory components, were vaporized in the innermost disk region, bounded by the so-called 'tar line' or 'soot line'. This scenario is supported by high-vacuum heating experiments, which show that interstellar organic analogs can persist at temperatures up to ~ 350–450 K (Nakano et al., 2003), as well as by theoretical estimates of the sublimation temperatures of carbonaceous organics (~500 K; Li et al., 2021). Consequently, sunward of the tar line, the dominant N sources available to accreting planetesimals were likely restricted to the most refractory organic compounds or thermally-processed residues (Fig. 5). In addition, thermal decomposition of more labile organics may have locally increased the gas-phase C/O ratio (Righter et al., 2016), promoting reducing conditions favorable to the formation and preservation of reduced phases such as nitrides. Such 'solar' nitrides—characterized by isotopically light N isotopic compositions ($\delta^{15}N = -60$ ‰; Leitner et al., 2018)—may have served as an additional N source for the parent bodies of enstatite chondrites (Grady et al., 1986; Rubin, 1997). Importantly, the tar line is thought to have initially been located several, possibly up to several tens, of au from the Sun, but

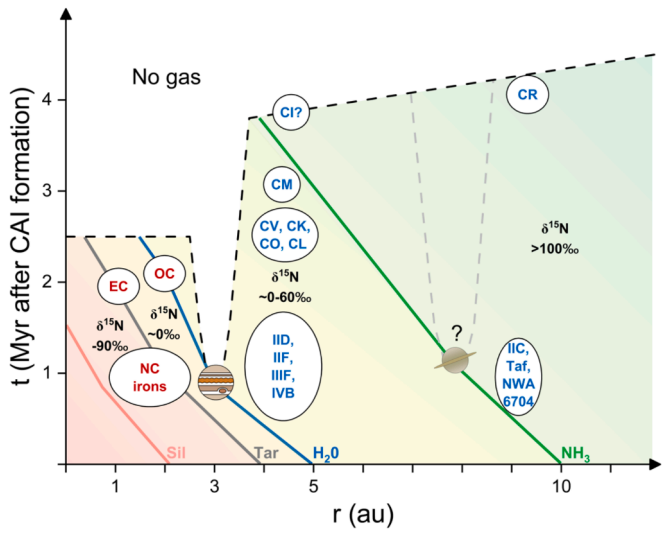

Fig. 5. Schematic evolution of the protoplanetary disk showing the inward migration of the silicate (Sil), tar (Tar), and the water (H_2O) and ammonia (NH_3) ice sublimation lines. The horizontal axis denotes heliocentric distance, and the vertical axis denotes time after calcium-aluminum-rich inclusions (CAIs). Also indicated are the potential formation zones of the parent bodies of NC and CC meteorites, together with their predominant $\delta^{15}N$ ranges. At present, it remains unclear whether iron meteorite parent body formation in the outer disk was triggered by the rapid growth of the gas giant cores or by other disk substructures, such as the water snowline. Likewise, the formation location of the CI parent body or bodies remains debated, with proposed heliocentric distances ranging from $\leq$ 5 to beyond $\sim$ 15 au (e.g., Desch et al., 2018; Hopp et al., 2022; Spitzer et al, 2024; Genge et al., 2025). Taf: Tafassasset-related ungrouped primitive carbonaceous achondrites; NWA 6704: NWA 6704-related ungrouped pyroxenitic achondrites.

migrated inward over time, eventually passing within 1 au (Yang et al., 2013; Li et al., 2021; Desch et al., 2018) (Fig. 5). As a result, organics in the inner disk were likely at least partially destroyed within the first 1 Myr of Solar System formation (Bermingham et al. 2020; Li et al. 2021). It is therefore plausible that these N-bearing components, particularly the ^{15}N-rich, labile ones, were less abundant during the accretion of NC iron meteorite parent bodies, resulting in their ^{15}N-depleted isotopic signatures compared to NC chondrites.

Overall, the distinct N isotopic compositions of NC iron meteorites and chondrites may reflect the spatiotemporal variability of isotopically different N-bearing phases or components that were stable in the inner protoplanetary disk. Early-formed iron meteorite parent bodies appear to have accreted smaller proportions of ^{15}N-rich, thermally labile components than later-forming chondrite parent bodies, possibly as a result of the inward migration of the tar line (Fig. 5). Notably, because evaporation fronts such as the tar line were diffuse (e.g., Boitard-Crépeau et al., 2025), and because the spatiotemporal distribution of N carriers would not only have depended on the evolving thermal structure of the disk but also on the extent of radial and vertical mixing of gas and solids (Kress et al., 2010), some N isotopic heterogeneity among NC iron meteorite parent bodies cannot be ruled out. In contrast, dust grains carrying more refractory elements were largely unaffected by the tar line; consequently, both early-formed differentiated bodies and late-formed chondritic planetesimals in the NC reservoir have similar signatures in the nucleosynthetic anomalies that define the NC-CC isotopic dichotomy.

4.3. Accretionary relationships and evolution of the CC reservoir traced by $\delta^{15}N$

4.3.1. Isotopic constraints on genetic relationships among CC meteorites

Most grouped (IID, IIF, IIIF, IIC) and ungrouped CC iron meteorites record positive $\delta^{15}N$ values (Fig. 1**b** and Fig. 4). This suggests that the inferred formation of their parent bodies at greater heliocentric distances, presumably beyond the tar line (Fig. 5) and Jupiter (Kruijer et al., 2017), permitted the accretion of a greater proportion of ^{15}N-enriched precursors compared to the parent bodies of the NC magmatic iron meteorite groups (Grewal et al., 2021b, 2025). Among these, the IIC group stands out with particularly high $\delta^{15}N$ values ($\delta^{15}N_{IIC}$ = +125 to +163 ‰; Franchi et al., 1993; Prombo and Clayton, 1993; Sugiura, 1998), comparable to those of CR chondrites ($\delta^{15}N_{CR}$ predominantly between +135 and 190 ‰; Kung and Clayton, 1978; Robert and Epstein, 1982; Grady et al., 1983; Kerridge, 1985; Pearson et al., 2006; Alexander et al., 2012, 2013) (Fig. 1**b**). In addition to their similar N isotopic compositions, IIC irons and CR chondrites also share nucleosynthetic anomalies in Mo, W, Fe, and Ni (Budde et al., 2018; Spitzer et al., 2025a, b). In this study, three CC ungrouped irons—New Baltimore (+104 ‰), Hammond (+112 ‰), and La Caille (+206 ‰) (Fig. 4)—were found to have high $\delta^{15}N$ values comparable to those of IIC irons and CR chondrites. Complementary Mo, Fe, and Ni isotope data confirm their CR-like isotopic signatures (Spitzer et al., 2025b), reinforcing a genetic link between these ungrouped irons and the IIC/CR reservoir.

To investigate this relationship in more detail, we performed a hierarchical clustering analysis of N isotopic compositions and isotope anomalies of CC meteorites based on Gower dissimilarities (Gower, 1971) (Supplementary Table S2 and Fig. 6). The resulting dendrogram can be interpreted as a genetic family tree of CC meteorites and reveals a primary divide between Ivuna-type (CI) carbonaceous chondrites and CI-like materials (Ryugu, Bennu, and Yamato-type (CY1) chondrites), on the one hand, and all non-CI meteorites on the other. The unique isotopic heritage of CI chondrites has been recognized previously (Hopp et al., 2022; Dauphas et al., 2024; Spitzer et al., 2024), and our analysis confirms that they have no differentiated genetic equivalent. This finding reinforces the hypothesis that CI parent bodies formed through a unique mechanism or in a unique environment (Spitzer et al., 2024) (see **Section 4.3.3**.). The dissimilarity analysis further subdivides the non-CI meteorites into two clusters: CV-CK-CO-like (Vigarano-, Karoonda-, and Ornans-type carbonaceous chondrites) and CR-like.

The CV-CK-CO-like and CR-like clusters are populated by both undifferentiated and differentiated meteorites, providing evidence that planetesimals with these two isotopic signatures—representing specific material mixtures—accreted over an extended period within the outer disk. CV-CK-CO chondrites are characterized by high abundances of refractory inclusions (CAIs and amoeboid olivine aggregates, AOAs) and chondrules, and thus have low matrix content, whereas CR chondrites are depleted in refractory inclusions (Rubin, 2011). Early-formed (differentiated) bodies in the two genetic clusters are therefore expected to have accreted from similarly contrasting material mixtures. However, quantifying the refractory material accreted by iron meteorite parent bodies can only be achieved indirectly, and the results depend strongly on the modeled S content of their cores (Spitzer et al., 2025a). Nevertheless, the three CC iron meteorite groups IID, IIF, and IIIF fall within the CV-CK-CO-like cluster (Fig. 6); they are therefore interpreted to derive from parent bodies rich in refractory inclusions (and chondrules) but relatively poor in matrix, and the clustering implies planetesimal formation within a common source reservoir and/or from similar precursor materials. The CAI-poor nature inferred for the IIC irons (Zhang et al., 2024) is consistent with their affiliation with the CR-like cluster.

Spitzer et al. (2025b) previously suggested that many differentiated CC meteorites may be related to the CR reservoir, a relationship that is now supported by a larger and more robust dataset (Supplementary Table S2 and Fig. 6). Notably, the CR cluster identified in this study and in Spitzer et al. (2025b) includes irons with elevated $\delta^{15}N$ values (New Baltimore, Hammond, and La Caille) but also some with comparatively low $\delta^{15}N$ values, ranging from –10 to +49 ‰ (this study; Prombo and Clayton, 1993) (Fig. 4). These low-$\delta^{15}N$ irons are moderately (Illinois Gulch, Nordheim) to severely Ge-depleted (Guffey,

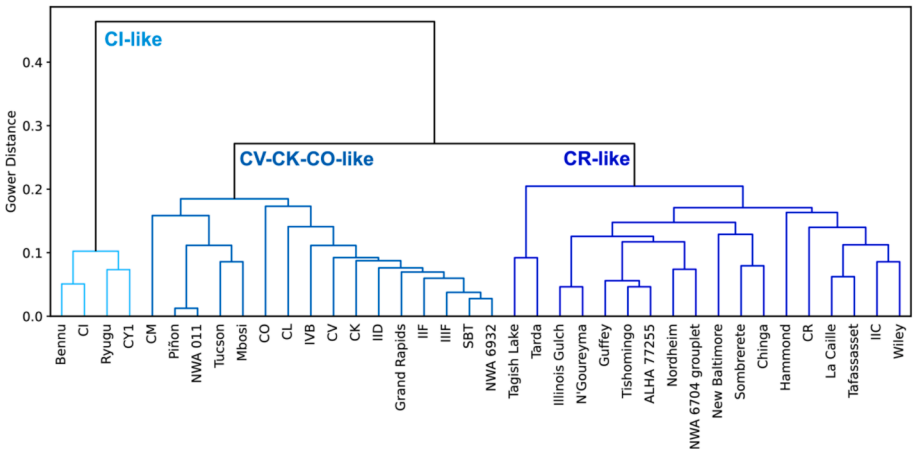

Fig. 6. Dendrogram from agglomerative hierarchical clustering (average linkage) of CC meteorites (iron meteorites, chondrites, and the ungrouped achondrites Tafassasset, NWA 011, and the NWA 6704 grouplet) and samples returned from Ryugu and Bennu, computed using Gower dissimilarities of multiple isotopic ratios (δ^{15}N and Δ^{17}O, ε^{50}Ti, ε^{54}Cr, μ^{54}Fe, μ^{60}Ni, μ^{64}Ni, ε^{94}Mo, Δ^{95}Mo, ε^{100}Ru) as reported in Supplementary Table S2. Pairwise dissimilarities were calculated as the mean absolute difference of range-normalized variables, using only variables measured for both samples (i.e., excluding missing values on a pairwise basis). Branch length is proportional to Gower dissimilarity (0 = identical; 1 = maximally different). For sample pairs sharing data for only one or two isotopic variables, the raw Gower distance may become artificially small and dominate the clustering despite being poorly constrained. To mitigate this effect, a mild distance penalization (penalty factor = 1.2) was applied to pairwise comparisons based on fewer than three shared variables. This approach reduces spurious clustering driven by single-variable overlap while preserving the overall cluster structure. Importantly, the penalization affects only sparsely constrained comparisons and does not alter the clustering of well-characterized samples. The dendrogram was cut at $k = 3$ to highlight the three major clusters corresponding to the CI-, CV–CK–CO–, and CR-like groups (clusters shown in different shades of blue). Data sources: N in Ryugu samples (Nakamura et al., 2022; Naraoka et al., 2023; Oba et al., 2023; Gamblin et al., 2024); N in Bennu samples (Lauretta et al., 2024; Barnes et al., 2025; Marty et al., 2025; Glavin et al., 2025); N in chondrites (Injerd and Kaplan, 1974; Kung and Clayton, 1978; Thiemens and Clayton, 1981; Robert and Epstein, 1982; Grady et al., 1983, 2002; Lewis et al., 1983; Kerridge, 1985; Sephton et al., 2003; Pearson et al., 2006; Alexander et al., 2012, 2018, 2013; Füri et al., 2013; Marrocchi et al., 2021; Hashizume et al., 2024; Patzek et al., 2025); N in iron meteorites (this study; Pepin and Becker, 1982; Prombo and Clayton, 1993; Grewal et al., 2021b); Ni (Spitzer et al., 2024, Spitzer et al., 2025b); Fe (Hopp et al., 2022; Anand et al., 2024; Spitzer et al., 2025b); Mo (Spitzer et al., 2025a); Ru, Ti, Cr (Tissot et al., 2025); O (Spitzer et al., 2025b).

N'Goureyma, Tishomingo, and ALHA 77255); consequently, as discussed in **Section 4.1.**, the N isotopic compositions of these specimens may have been modified by volatile loss and therefore may not faithfully record parent-body-specific source signatures. Fig. 6 also illustrates that some Tafassasset-related ungrouped primitive carbonaceous achondrites (Ma et al., 2022) and NWA 6704-related ungrouped pyroxenitic achondrites (Hibiya et al., 2019; Sanborn et al., 2019) are thought to have accreted within the CR reservoir (Ma et al., 2022; Spitzer et al., 2025b), whereas the NWA 011-related ungrouped basaltic achondrites (e.g., Ma et al., 2022) falls within the CV-CK-CO-like cluster. However, no N isotopic data are yet available for these specimens. These achondrites therefore represent promising targets for future studies aimed at refining our understanding of planetesimal formation and N accretion within the CC reservoir.

4.3.2. *Evidence for a long-lived, high δ^{15}N outer disk reservoir*

CR chondrites are characterized by a suite of petrological and isotopic features that collectively define an outer-disk reservoir, chemically and isotopically distinct from the other CC sub-reservoirs (Figs. 5 and 6; Spitzer et al., 2024; Shollenberger et al., 2025). They contain the most primitive and least-altered ^{15}N-rich (insoluble) organic matter (Alexander et al., 1998), which is thought to have formed in the interstellar medium or outer Solar System. These organics can reach δ^{15}N values of up to +300 ‰ (Alexander et al., 2007) and contain localized ^{15}N 'hotspots' with δ^{15}N values as high as +1500 to 2000 ‰ (Busemann et al., 2006). In addition to their ^{15}N-enrichment, CR chondrites record highly elevated D/H ratios compared to almost all other carbonaceous chondrites (Alexander et al., 2012; Broadley et al., 2022), as well as low abundances of refractory inclusions (Rubin, 2011) but high abundances of presolar grains (Leitner et al., 2012). A unique formation setting is further supported by chronological evidence from chondrule ages: CR chondrites appear to have formed significantly later than other chondrite groups, ~4 Myr after CAIs (Schrader et al., 2017; Budde et al., 2018; Neumann et al., 2024), and two major chondrule formation episodes at 2.5 ± 0.3 Ma and 3.8 ± 0.3 Ma after CAI formation (Tenner et al., 2019; Marrocchi et al., 2022) point to a long-lived, isotopically isolated reservoir. Taken together, these lines of evidence suggest that the parent body (or bodies) of CR chondrites accreted in a spatially and/or temporally separate region of the disk compared to those of other chondrite groups (Fig. 5).

Recently, the matrices of some CR chondrites were found to host abundant dark inclusions or clasts composed of CI-like fine-grained material, organics, and up to 10 vol% of chondrules, occurring as pebbly aggregates (Van Kooten et al., 2024; Hewins et al., 2025). These clasts contain magnetite with framboidal and plaquette textures that indicate formation under alkaline, NH_3-rich fluid conditions (Harju et al., 2014; Singerling and Brearley, 2020; Sridhar et al., 2021), consistent with the accretion of ammonia ice in addition to water ice (Van Kooten et al., 2024; Hewins et al., 2025). The high δ^{15}N values and elevated D/H ratios of bulk CR chondrites and their components—far exceeding those of inner-disk materials—further support an origin in a cold, ammonia-ice-bearing region of the disk, possibly linked to the formation zone of cometary material (Pizzarello and Williams, 2012; Alexander et al., 2012; Piani et al., 2021; Van Kooten et al., 2024; Hewins et al., 2025), with photodissociation-driven N isotope fractionation at the disk surface (self-shielding or peculiar quantum effects) providing a mechanism for generating the associated ^{15}N-rich ices or organics (Füri and Marty, 2015; Van Kooten et al., 2024, and references therein). Independent support for such an ammonia-rich reservoir comes from reflectance spectra of asteroids displaying a broad 3.2 μm absorption feature diagnostic of NH_3-bearing ices (e.g., the 'not-sharp-type' class and comet 67P) (Poch et al., 2020; Rivkin et al., 2022).

In contrast to the late formation of the CR chondrite parent body (or bodies), differentiated planetesimals—such as the parent bodies of the ^{15}N-rich IIC irons and the CC ungrouped irons studied here—accreted within the first ~ 1.5 Myr after CAIs (Kruijer et al., 2017; Spitzer et al., 2021, Spitzer et al., 2025a; Bryson et al., 2026) (Fig. 5). This temporal offset implies that the isotopically CR-like, ammonia-rich

reservoir was established shortly after CAI formation and persisted for several million years of disk evolution. Thus, mineralogical and isotopic evidence across a range of planetesimals—including differentiated bodies sampled by IIC and CC ungrouped irons, as well as undifferentiated materials such as CR chondrites—supports the presence of ammonia ice in an outer disk reservoir characterized by elevated $\delta^{15}N$ values. Despite this evidence, the distribution, stability, and persistence of ammoniated ice within the early protoplanetary disk, and its role in planetesimal formation, remain uncertain. Constraining the spatiotemporal distribution of ammoniated ice in meteorite parent bodies is therefore essential, as it could provide key insights into distinct planetesimal formation environments in the early Solar System.

4.3.3. NH_3 ice line migration and implications for NH_3 accretion

Disk-evolution models tailored to the early Solar System place the ammonia ice line at approximately 9–12 au during the late stages of disk dispersal (Chen et al., 2019), migrating inward as accretion diminished. These distances lie well beyond the H_2O snowline, which exerted the dominant control on ice mass and is commonly inferred to have been located at ~2–5 au early in disk history and to have contracted to ~1–2 au by ~ 3 Ma (Oka et al., 2011; Desch et al., 2018) (Fig. 5). Early- and late-formed parent bodies of IIC irons and CR chondrites, respectively, characterized by high $\delta^{15}N$ values, are therefore inferred to have accreted farther from Jupiter than planetesimals sampled by other chondrite groups, which contain isotopically lighter N (Fig. 5). Notably, laboratory and theoretical studies indicate that NH_3 can be retained beyond its classical sublimation temperature through trapping in H_2O– and CO_2-rich ices, leading to secondary desorption fronts when the host ice sublimates (Bar-Nun et al., 1985; Collings et al., 2004; Simon et al., 2019; Oberg et al., 2023). Inward-drifting icy pebbles may thus transport NH_3 past its nominal ice line (Piso et al., 2016; Oberg et al., 2023). Experimental and theoretical work further shows that hydrogen bonding between H_2O and NH_3 enhances NH_3 retention on icy grains to temperatures above 100 K, enabling ammonia ice to survive transport into warmer disk regions (Kruczkiewicz et al., 2021; Kakkenpara et al., 2024). Finally, ammonium salts represent an additional solid N reservoir that is more thermally stable than free NH_3 and may have enabled N delivery interior to the nominal NH_3 ice line (Lodders, 2004; Poch et al., 2020; Kruczkiewicz et al., 2021). Collectively, these constraints imply that the distribution and effective accretion of NH_3 ice in the outer protoplanetary disk were likely more complex than predicted by a single, sharply defined NH_3 ice line. Future high-resolution analyses, such as chemical separation or stepped-heating experiments, may help determine whether other chondrite groups (and irons) also contain traces of a ^{15}N-rich component derived from NH_3 accretion.

CI chondrites may represent key samples for addressing this complexity. Despite abundant mineralogical and petrographic evidence for ammonia-influenced aqueous alteration—including magnetite morphologies indicative of alkaline, NH_3-rich fluids (Sridhar et al., 2021)—CI chondrites, as well as samples returned from Ryugu and Bennu, record lower bulk $\delta^{15}N$ values than CR chondrites (Fig. 1**b**). While recent chemical separation and stepped-heating experiments on Orgueil and Bennu samples demonstrate the presence of an isotopically heavy, likely ammonia-derived N component in CI materials, with $\delta^{15}N$ values on the order of +160 to +180 ‰ (Laize-Générat et al., 2024; Marty et al., 2025; Glavin et al., 2025), the comparatively low bulk $\delta^{15}N$ values of CI chondrites suggests that their parent body or bodies accreted sunward of those of CR chondrites and IID irons. This would imply incorporation of a smaller proportion of ^{15}N-enriched NH_3 ice relative to H_2O ice, with bulk $\delta^{15}N$ further diluted by additional N carriers. Although the CI parent body or bodies are commonly inferred to have accreted in the outermost disk (e.g., Desch et al., 2018; Hopp et al., 2022), emerging constraints instead suggest a formation location closer to the Sun (Spitzer et al, 2024; Genge et al., 2025) (Fig. 5). This may reflect formation through a unique mechanism or within a unique nebular environment, possibly related to photoevaporation at the end of the disk's lifetime (Spitzer et al., 2024), and may also be consistent with the apparent absence of differentiated genetic equivalents to CI chondrites (Fig. 6). Such a scenario is consistent with the framework outlined here, in which N isotopes serve as tracers of NH_3 ice line migration and NH_3 accretion.

5. Conclusions

The N isotopic compositions of NC and CC ungrouped magmatic iron meteorites, together with those from established magmatic groups, reveal a wider range of N isotopic variability present during the earliest stages of protoplanetary disk evolution and planetary accretion than is recorded by later-formed chondritic bodies. Whereas the isotopic dichotomy observed for elements with nucleosynthetic anomalies was primarily carried by refractory materials, N was predominantly hosted in organics and ice(s), with minor contributions from reduced phases such as nitrides, carbides, graphite. Consequently, the spatial and temporal distribution of N in the early disk was likely governed by the evolving thermal structure of the disk, which controlled the stability, transport, and incorporation of these volatile and refractory N carriers. Redox conditions may have further influenced the stability and retention of reduced N-bearing phases in the inner disk.

Most NC and CC iron meteorite groups show distinct N isotopic compositions, though some overlap remains—notably, when the IVA and IVB irons are considered. It is currently unclear whether the N isotopic compositions of these highly volatile-depleted samples reflect primary signatures of their parent planetesimals at the time of alloy-silicate separation or result from secondary modifications due to volatile loss. Nevertheless, the ^{15}N-depleted isotopic signatures of NC iron meteorite parent bodies suggest formation sunward of the tar line, where only the most refractory (organic) compounds or thermally-processed residues could have served as N sources for accreting planetesimals. In this context, the distinct N isotopic composition of NC iron meteorites and chondrites likely reflects the spatiotemporal variability of isotopically distinct N-bearing phases or components that were stable in the inner protoplanetary disk.

In contrast, the convergence of multiple lines of evidence—including petrographic textures (dark inclusions and framboidal magnetite), ammonia-driven alteration pathways, elevated $\delta^{15}N$ values and D/H ratios, low abundances of refractory-inclusions, and coherent nucleosynthetic signatures (e.g., Mo, Fe, and Ni isotopes) across CR chondrites, IIC irons, and newly analyzed CC ungrouped irons—points to the existence of a distinct, ammonia-rich outer-disk substructure. This reservoir was established within the first ~ 1 Myr of disk evolution and persisted for ~ 3–4 Myr, allowing both differentiated and undifferentiated chondritic planetesimals to inherit its distinctive ^{15}N-enriched isotopic signature. The high $\delta^{15}N$ values of the CC ungrouped irons further corroborate their genetic link to the IIC/CR reservoir and also illustrate how spatial and temporal disk substructures—perhaps sculpted by nascent giant planets—governed the heterogeneous distribution of ammonia-derived N, and, ultimately, divergent accretion and differentiation pathways among early-formed planetary bodies. Unlike the CI parent body or bodies, which likely accreted under conditions characterized by reduced incorporation of ^{15}N-rich NH_3, CR- and IIC-related materials preserve the signature of more efficient ammonia ice accretion.

CRediT authorship contribution statement

Evelyn Füri: Writing – original draft, Writing – review & editing, Supervision, Methodology, Investigation, Funding acquisition, Formal analysis, Data curation, Conceptualization. **Fridolin Spitzer:** Writing – original draft, Writing – review & editing, Visualization, Investigation. **Julie Gamblin:** Investigation. **Christoph Burkhardt:** Writing – original draft, Writing – review & editing, Resources, Conceptualization. **Béatrice Luais:** Writing – original draft, Writing – review & editing,

Resources. **Julien Boulliung:** Methodology. **Laurent Zimmermann:** Methodology.

Declaration of competing interest

The authors declare that they have no known competing financial interests or personal relationships that could have appeared to influence the work reported in this paper.

Acknowledgements

We thank the Field Museum (Chicago), the Naturhistorisches Museum (Vienna), the Muséum National d'Histoire Naturelle (Paris), the Natural History Museum (London), the Smithsonian Institution, the Naturhistorisches Museum (Bern), and the Institut für Planetologie (Münster) for generously providing meteorite samples for this study. Special thanks go to Bouchaib Tibari and Allan Bauer for assistance with the noble gas analyses at CRPG, and to Louna Perez (MNHN) and Joanna Drążkowska (MPS) for fruitful discussions. We are also grateful to the constructive reviews provided by Ko Hashizume and two anonymous reviewers, and to Eric Quirico for editorial handling. This work was funded by the European Union (ERC, IRONIS, 101087562, awarded to E. F.). Views and opinions expressed are however those of the author(s) only and do not necessarily reflect those of the European Union or the European Research Council. Neither the European Union nor the granting authority can be held responsible for them. This is CRPG contribution 2884.

Appendix A. Supplementary material

Supplementary material associated with this article contains the N–Ne–Ar abundances and isotope ratios of the iron meteorites analyzed in this study, as well as the isotopic datasets used for hierarchical clustering of outer-disk meteorite samples and their corresponding cluster assignments. Supplementary material to this article can be found online at https://doi.org/10.1016/j.gca.2026.05.037.

Data availability

The compiled N isotopic compositions and abundances of iron meteorites (from stepped heating or fusion analyses) and chondrites are available through ORDaR (OTELo Research Data Repository) at https://doi.org/10.24396/ORDAR-185 and https://doi.org/10.24396/ORDAR-190, respectively. N–Ne–Ar data from this study, as well as the isotopic data used for the hierarchical clustering analysis, are available through ORDaR at https://doi.org/10.24396/ORDAR-191.

References

Alexander, C.M.O'D., Greenwood, R.C., Bowden, R., Gibson, J.M., Howard, K.T., Franchi, I.A., 2018. A multi-technique search for the most primitive CO chondrites. Geochim. Cosmochim. Acta 221, 406–420.

Alexander, C.M.O'D., Howard, K.T., Bowden, R., Fogel, M.L., 2013. The classification of CM and CR chondrites using bulk H, C and N abundances and isotopic compositions. Geochim. Cosmochim. Acta 123, 244–260.

Alexander, C.M.O'D., Bowden, R., Fogel, M.L., Howard, K.T., Herd, C.D.K., Nittler, L.R., 2012. The provenances of asteroids, and their contributions to the volatile inventories of the terrestrial planets. Geochim. Cosmochim. Acta 337, 721–723.

Alexander, C.M.O'D., Fogel, M., Yabuta, H., Cody, G.D., 2007. The origin and evolution of chondrites recorded in the elemental and isotopic compositions of their macromolecular organic matter. Geochim. Cosmochim. Acta 71, 4380–4403.

Alexander, C.M.O'D., Russell, S.S., Arden, J.W., Ash, R.D., Grady, M.M., Pillinger, C.T., 1998. The origin of chondritic macromolecular organic matter: a carbon and nitrogen study. Meteorit. Planet. Sci. 33, 603–622.

Anand, A., Spitzer, F., Hopp, T., Windmill, R., Kruttasch, P., Burkhardt, C., Dauphas, N., Greenwood, R., Hofmann, B., Mezger, K., Kleine, T., 2024. Isotopic evidence for a common parent body of IIG and IIAB iron meteorites. Geochim. Cosmochim. Acta 382, 118–127.

Anders, E., Grevesse, N., 1989. Abundances of the elements: meteoritic and solar. Geochim. Cosmochim. Acta 53, 197–214.

Asphaug, E., 2010. Similar-sized collisions and the diversity of planets. Geochem 70, 199–219.

Barnes, J.J., Nguyen, A.N., Abernethy, F.A.J., Bajo, K., Bekaert, D.V., Bloch, E., Brennecka, G.A., Busemann, H., Cowpe, J.S., Crowther, S.A., Ek, M., Fawcett, L.J., Fehr, M.A., Franchi, I.A., Füri, E., Gilmour, J.D., Grady, M.M., Greenwood, R.C., Haenecour, P., Kawasaki, N., Koefoed, P., Krietsch, D., Le, L., Liszewska, K.M., Maden, C., Malley, J., Marrocchi, Y., Marty, B., Meyer, L.A.E., Peretyazhko, T.S., Piani, L., Render, J., Russell, S.S., Rüfenacht, M., Sakamoto, N., Schönbächler, M., Shollenberger, Q.R., Smith, L., Thomas-Keprta, K., Verchovsky, A.B., Villeneuve, J., Wang, K., Welten, K.C., Wimpenny, J., Worsham, E.A., Yurimoto, H., Zimmermann, L., Zhao, X., Alexander, C.M.O'D., Amini, M., Baczynski, A., Bland, P., Borg, L.E., Burgess, R., Caffee, M.W., Chaves, L.C., Clay, P.L., Dworkin, J.P., Foustoukos, D.I., Glavin, D.P., Hamilton, V.E., Hill, D., House, C.H., Huss, G.R., Ireland, T., Jilly, C.E., Jourdan, F., Keller, L.P., Kruijer, T.S., Lai, V., McCoy, T.J., Nagashima, K., Nishiizumi, K., Ogliore, R., Ong, I.J., Reddy, S.M., Rickard, W.D.A., Sandford, S., Saxey, D.W., Timms, N., Weis, D., Wilbur, Z.E., Zega, T.J., DellaGiustina, D.N., Wolner, C.W.V., Connolly, H.C., Lauretta, D.S., 2025. The variety and origin of materials accreted by Bennu's parent asteroid. Nat. Astron 9, 1785–1802.

Bar-Nun, A., Hermann, G., Laufer, D., 1985. Trapping and release of gases by water ice and implications for icy bodies. Icarus 63, 317–332.

Becker, R.H., Pepin, R.O., 1987. Solar composition noble gases in the Washington County iron meteorite: a correction. Earth Planet. Sci. Lett. 84, 356.

Belai, H., Hanson, A.L., Jones, K.W., 1995. Application of $^{14}N(d,\alpha)^{12}C$ nuclear reaction to the concentration analysis of nitrogen in iron meteorites. Chin. Phys. Lett. 12, 265–268.

Benedix, G.K., Haack, H., McCoy, T.J., 2013. Iron and stony-iron meteorites. In Treatise on Geochemistry: 2nd Edition Elsevier Ltd., Kidlington, Oxford, UK: Elsevier Science BV. pp. 267–285.

Benedix, G.K., McCoy, T.J., Keil, K., Love, S.G., 2000. A petrologic study of the IAB iron meteorites: constraints on the formation of the IAB-Winonaite parent body. Meteorit. Planet. Sci. 35, 1127–1141.

Bermingham, K.R., Füri, E., Lodders, K., Marty, B., 2020. The NC-CC isotope dichotomy: implications for the chemical and isotopic evolution of the early solar system. Space Sci. Rev. 216, 133.

Bermingham, K.R., Worsham, E.A., Walker, R.J., 2018. New insights into Mo and Ru isotope variation in the nebula and terrestrial planet accretionary genetics. Earth Planet. Sci. Lett. 487, 221–229.

Black, D., 1972. On the origins of trapped helium, neon and argon isotopic variations in meteorites—I. Gas-rich meteorites, lunar soil and breccia. Geochim. Cosmochim. Acta 36, 347–375.

Boitard-Crépeau, L., Ceccarelli, C., Beck, P., Vacher, L., Ugliengo, P., 2025. Was earth's water acquired locally during the earliest phases of the solar system formation? Astrophys. J. Lett. 987, L25.

Bouvier, A., Bermingham, K.R., Füri, E., 2025. Planetary materials: A record of early Solar System events to planetary processes. In Treatise on Geochemistry (eds. D. Weis and A. Anbar). Elsevier. pp. 203–256.

Broadley, M.W., Byrne, D.J., Füri, E., Zimmermann, L., Marty, B., Okazaki, R., Yada, T., Kitajima, F., Tachibana, S., Yogata, K., Sakamoto, K., Yurimoto, H., Nakamura, T., Noguchi, T., Naraoka, H., Yabuta, H., Watanabe, S., Tsuda, Y., Nishimura, M., Nakato, A., Miyazaki, A., Abe, M., Okada, T., Usui, T., Yoshikawa, M., Saiki, T., Tanaka, S., Terui, F., Nakazawa, S., Busemann, H., Hashizume, K., Gilmour, J.D., Meshik, A., Riebe, M.E.I., Krietsch, D., Maden, C., Ishida, A., Clay, P., Crowther, S.A., Fawcett, L., Lawton, T., Pravdivtseva, O., Miura, Y.N., Park, J., Bajo, K., Takano, Y., Yamada, K., Kawagucci, S., Matsui, Y., Yamamoto, M., Righter, K., Sakai, S., Iwata, N., Shirai, N., Sekimoto, S., Inagaki, M., Ebihara, M., Yokochi, R., Nishiizumi, K., Nagao, K., Lee, J.I., Kano, A., Caffee, M.W., Uemura, R., 2023. The noble gas and nitrogen relationship between Ryugu and carbonaceous chondrites. Geochim. Cosmochim. Acta 345, 62–74.

Broadley, M.W., Bekaert, D.V., Piani, L., Füri, E., Marty, B., 2022. Origin of life-forming volatile elements in the inner Solar System. Nature 611, 245–255.

Bryson, F.J., Sanderson, H.R., Nimmo, F., Sridhar, S., Brennecka, G.A., Marrocchi, Y., Terry, J.P., 2026. A collective trigger for widespread planetesimal formation revealed by accretion ages. Earth Planet. Sci. Lett. 681, 119936.

Buchwald, V.F., 1975. Handbook of iron meteorites. Their History, Distribution, Composition and Structure. University of California Press.

Buchwald, V.F., Scott, E.R.D., 1971. First nitride (CrN) in iron meteorites. Nat. Phys. Sci. 233, 113–114.

Budde, G., Kruijer, T.S., Kleine, T., 2018. Hf-W chronology of CR chondrites: implications for the timescales of chondrule formation and the distribution of 26Al in the solar nebula. Geochim. Cosmochim. Acta 222, 284–304.

Budde, G., Burkhardt, C., Brennecka, G.A., Fischer-Gödde, M., Kruijer, T.S., Kleine, T., 2016. Molybdenum isotopic evidence for the origin of chondrules and a distinct genetic heritage of carbonaceous and non-carbonaceous meteorites. Earth Planet. Sci. Lett. 454, 293–303.

Burkhardt, C., Kleine, T., Oberli, F., Pack, A., Bourdon, B., Wieler, R., 2011. Molybdenum isotope anomalies in meteorites: constraints on solar nebula evolution and origin of the Earth. Earth Planet. Sci. Lett. 312, 390–400.

Busemann, H., Young, A.F., Alexander, C.M.O'D., Hoppe, P., Mukhopadhyay, S., Nittler, L.R., 2006. Interstellar chemistry recorded in organic matter from primitive meteorites. Science 312, 727–730.

Campbell, A.J., Humayun, M., 2005. Compositions of group IVB iron meteorites and their parent melt. Geochim. Cosmochim. Acta 69, 4733–4744.

Chabot, N.L., 2004. Sulfur contents of the parental metallic cores of magmatic iron meteorites. Geochim. Cosmochim. Acta 68, 3607–3618.

Chan, Q.H.S., Chikaraishi, Y., Takano, Y., Ogawa, N.O., Ohkouchi, N., 2016. Amino acid compositions in heated carbonaceous chondrites and their compound-specific nitrogen isotopic ratios. Earth Planet. Sp. 68, 7.

Chen, C., Smallwood, J.L., Martin, R.G., Livio, M., 2019. Late delivery of nitrogen to Earth. AJ 157, 80.

Collings, M.P., Anderson, M.A., Chen, R., Dever, J.W., Viti, S., Williams, D.A., McCoustra, M.R.S., 2004. A laboratory survey of the thermal desorption of astrophysically relevant molecules. MNRAS 354, 1133–1140.

Corrigan, C.M., Nagashima, K., Hilton, C., McCoy, T.J., Ash, R.C., Tornabene, H.A., Walker, R.J., McDonough, W.F., Rumble, D., 2022. Nickel-rich, volatile depleted iron meteorites: relationships and formation processes. Geochim. Cosmochim. Acta 333, 1–21.

Dalou, C., Füri, E., Deligny, C., Piani, L., Caumon, M.-C., Laumonier, M., 2019. Redox control on nitrogen isotope fractionation during planetary core formation. PNAS 116, 14485–14494.

Dauphas, N., Hopp, T., Nesvorný, D., 2024. Bayesian inference on the isotopic building blocks of Mars and Earth. Icarus 408, 115805.

Desch, S.J., Dunlap, D.R., Williams, C.D., Mane, P., Dunham, E.T., 2023. Statistical chronometry of meteorites: II. Initial abundances and homogeneity of short-lived radionuclides. Icarus 402, 115611.

Desch, S.J., Kalyaan, A., Alexander, C.M., O'd., 2018. The effect of Jupiter's formation on the distribution of refractory elements and inclusions in meteorites. ApJS 238, 11.

Eberhardt, P., Eugster, O., Marti, K., 1965. A redetermination of the isotopic composition of atmospheric neon. Z. Naturforsch. 20, 623–624.

Fegley Jr., B., 1983. Primordial retention of nitrogen by terrestrial planets and meteorites. J. Geophys. Res. Solid Earth 88, A853–A868.

Florin, G., Luais, B., Alard, O., Rushmer, T., 2021. Condensation and evaporation processes during CB chondrite formation: insights from Ge isotopes and highly siderophile element abundances. Meteorit. Planet. Sci. 56, 1191–1211.

Franchi, I.A., Wright, I.P., Pillinger, C.T., 1993. Constraints on the formation conditions of iron meteorites based on concentrations and isotopic compositions of nitrogen. Geochim. Cosmochim. Acta 57, 3105–3121.

Füri, E., Marty, B., 2015. Nitrogen isotope variations in the Solar System. Nat. Geosci. 8, 515–522.

Füri, E., Barry, P.H., Taylor, L.A., Marty, B., 2015. Indigenous nitrogen in the Moon: constraints from coupled nitrogen–noble gas analyses of mare basalts. Earth Planet. Sci. Lett. 431, 195–205.

Füri, E., Aléon-Toppani, A., Marty, B., Libourel, G., Zimmermann, L., 2013. Effects of atmospheric entry heating on the noble gas and nitrogen content of micrometeorites. Earth Planet. Sci. Lett. 377–378, 1–12.

Gamblin, J., Füri, E., Luais, B., Zimmermann, L., 2026. Nitrogen isotopic variations in the early Solar System recorded by pallasites. Geochem. Persp. Let. 39, 17–21.

Gamblin, J., Füri, E., Marty, B., Zimmermann, L., Bekaert, D.V., 2024. Dissecting the complex Ne-Ar-N signature of asteroid Ryugu by step-heating analysis. Geochem. Persp. Lett. 31, 44–48.

Genge, M.J., Almeida, N.V., van Ginneken, M., Pinault, L., Salge, T., Wozniakiewicz, P.J., Yano, H., Desch, S.J., 2025. Abundant microchondrules in 162173 Ryugu suggest a turbulent origin for primitive asteroids. Nat. Commun. 16, 6466.

Gibson, E.K., Moore, C.B., 1971. The distribution of total nitrogen in iron meteorites. Geochim. Cosmochim. Acta 35, 877–890.

Glavin, D.P., Dworkin, J.P., Alexander, C.M., O'd., et al., 2025. Abundant ammonia and nitrogen-rich soluble organic matter in samples from asteroid (101955) Bennu. Nat. Astron 9, 199–210.

Goel, P.S., 1970. Determination of nitrogen in iron meteorites. Geochim. Cosmochim. Acta 34, 932–935.

Goldstein, J.I., Huss, G.R., Scott, E.R.D., 2017. Ion microprobe analyses of carbon in Fe–Ni metal in iron meteorites and mesosiderites. Geochim. Cosmochim. Acta 200, 367–407.

Gower, J.C., 1971. A general coefficient of similarity and some of its properties. Biom 27, 857.

Grady, M.M., Wright, I.P., 2003. Elemental and isotopic abundances of carbon and nitrogen in meteorite. Space Sci. Rev. 106, 231–248.

Grady, M.M., Verchovsky, A.B., Franchi, I.A., Wright, I.P., Pillinger, C.T., 2002. Light element geochemistry of the Tagish Lake CI2 chondrite: comparison with CI2 and CM2 meteorites. Meteorit. Planet. Sci. 37, 713–735.

Grady, M.M., Wright, I.P., Carr, L.P., Pillinger, C.T., 1986. Compositional differences in enstatite chondrites based on carbon and nitrogen stable isotope measurements. Geochim. Cosmochim. Acta 50, 2799–2813.

Grady, M.M., Wright, I.P., Fallick, A.E., Pillinger, C.T., 1983. The stable isotopic composition of carbon, nitrogen and hydrogen in some Yamato meteorites. Proc. 8th Symp. Antarct. Meteorites, Mem. Natl. Inst. Polar Res. 30, 292–305.

Grewal, D.S., 2022. Origin of nitrogen isotopic variations in the rocky bodies of the solar system. ApJ 937, 123.

Grewal, D.S., Asimow, P.D., 2023. Origin of the superchondritic carbon/nitrogen ratio of the bulk silicate Earth – an outlook from iron meteorites. Geochim. Cosmochim. Acta 344, 146–159.

Grewal, D.S., Bhattacharjee, S., Mardaru, G.-D., Asimow, P.D., 2025. Tracing the origin of volatiles on Earth using nitrogen isotope ratios in iron meteorites. Geochim. Cosmochim. Acta 388, 34–47.

Grewal, D.S., Nie, N.X., Zhang, B., Izidoro, A., Asimow, P.D., 2024. Accretion of the earliest inner Solar System planetesimals beyond the water snowline. Nat. Astron 8, 290–297.

Grewal, D.S., Sun, T., Aithala, S., Taylor, H., Dasgupta, R., Yeung, L.Y., Schauble, E.A., 2022a. Limited nitrogen isotopic fractionation during core-mantle differentiation in rocky protoplanets and planets. Geochim. Cosmochim. Acta 338, 347–364.

Grewal, D.S., Seales, J.D., Dasgupta, R., 2022b. Internal or external magma oceans in the earliest protoplanets – perspectives from nitrogen and carbon fractionation. Earth Planet. Sci. Lett. 598, 117847.

Grewal, D.S., Dasgupta, R., Hough, T., Farnell, A., 2021a. Rates of protoplanetary accretion and differentiation set nitrogen budget of rocky planets. Nat. Geosci. 14, 369–376.

Grewal, D.S., Dasgupta, R., Marty, B., 2021b. A very early origin of isotopically distinct nitrogen in inner Solar System protoplanets. Nat. Astron 5, 356–364.

Györe, D., Tait, A., Hamilton, D., Suart, F., 2019. The formation of NeH^+ in static vacuum mass spectrometers and re-determination of $^{21}Ne/^{20}Ne$ of air. Geochim. Cosmochim. Acta 263, 1–12.

Haack, H., Scott, E.R.D., Love, S.G., Brearley, A.J., McCoy, T.J., 1996. Thermal histories of IVA stony-iron and iron meteorites: evidence for asteroid fragmentation and reaccretion. Geochim. Cosmochim. Acta 60, 3103–3133.

Harju, E.R., Rubin, A.E., Ahn, I., Choi, B.-G., Ziegler, K., Wasson, J.T., 2014. Progressive aqueous alteration of CR carbonaceous chondrites. Geochim. Cosmochim. Acta 139, 267–292.

Hashizume, K., Ishida, A., Chiba, A., Okazaki, R., Yogata, K., Yada, T., Kitajima, F., Yurimoto, H., Nakamura, T., Noguchi, T., Yabuta, H., Naraoka, H., Takano, Y., Sakamoto, K., Tachibana, S., Nishimura, M., Nakato, A., Miyazaki, A., Abe, M., Okada, T., Usui, T., Yoshikawa, M., Saiki, T., Terui, F., Tanaka, S., Nakazawa, S., Watanabe, S., Tsuda, Y., Broadley, M.W., Busemann, H., the Hayabusa2 Initial Analysis Volatile Team, 2024. The Earth atmosphere-like bulk nitrogen isotope composition obtained by stepwise combustion analyses of Ryugu return samples. Meteorit. Planet. Sci. 59, 2117–2133.

Hashizume, K.K., Suguira, N., Sugiura, N., 1995. Nitrogen isotopes in bulk ordinary chondrites. Geochim. Cosmochim. Acta 59, 4057–4069.

Heber, V.S., Wieler, R., Baur, H., Olinger, C., Friedmann, T.A., Burnett, D.S., 2009. Noble gas composition of the solar wind as collected by the Genesis mission. Geochim. Cosmochim. Acta 73, 7414–7432.

Hewins, R.H., Zanetta, P.-M., Leroux, H., Laforet, S., Guillou, C.L., Marinova, M., Pont, S., Zanda, B., Brunetto, R., Gattacceca, J., Sonzogni, C., Piani, L., Marrocchi, Y., 2025. Accretion of the anomalous CR2 chondrite Northwest Africa 14674: implications for the complexities of the CR parent bodies. Geochim. Cosmochim. Acta 402, 234–249.

Hibiya, Y., Archer, G.J., Tanaka, R., Sanborn, M.E., Sato, Y., Iizuka, T., Ozawa, K., Walker, R.J., Yamaguchi, A., Yin, Q.-Z., Nakamura, T., Irving, A.J., 2019. The origin of the unique achondrite Northwest Africa 6704: constraints from petrology, chemistry and Re–Os, O and Ti isotope systematics. Geochim. Cosmochim. Acta 245, 597–627.

Hintenberger, H., Schultz, L., Wänke, H., Weber, H., 1967. Helium- und neonisotope in eisenmeteoriten und der tritiumverlust in hexaedriten. Z. Naturforsch. 22, 780–787.

Hirschmann, M.M., Bergin, E.A., Blake, G.A., Ciesla, F.J., Li, J., 2021. Early volatile depletion on planetesimals inferred from C–S systematics of iron meteorite parent bodies. PNAS 118, e2026779118.

Hopp, T., Dauphas, N., Abe, Y., Aléon, J.O'D., Alexander, C.M.O'D., Amari, S., Amelin, Y., Bajo, K., Bizzarro, M., Bouvier, A., Carlson, R.W., Chaussidon, M., Choi, B.-G., Davis, A.M., Di Rocco, T., Fujiya, W., Fukai, R., Gautam, I., Haba, M.K., Hibiya, Y., Hidaka, H., Homma, H., Hoppe, P., Huss, G.R., Ichida, K., Iizuka, T., Ireland, T.R., Ishikawa, A., Ito, M., Itoh, S., Kawasaki, N., Kita, N.T., Kitajima, K., Kleine, T., Komatani, S., Krot, A.N., Liu, M.-C., Masuda, Y., McKeegan, K.D., Morita, M., Motomura, K., Moynier, F., Nakai, I., Nagashima, K., Nesvorný, D., Nguyen, A., Nittler, L., Onose, M., Pack, A., Park, C., Piani, L., Qin, L., Russell, S.S., Sakamoto, N., Schönbächler, M., Tafla, L., Tang, H., Terada, K., Terada, Y., Usui, T., Wada, S., Wadhwa, M., Walker, R.J., Yamashita, K., Yin, Q.-Z., Yokoyama, T., Yoneda, S., Young, E.D., Yui, H., Zhang, A.-C., Nakamura, T., Naraoka, H., Noguchi, T., Okazaki, R., Sakamoto, K., Yabuta, H., Abe, M., Miyazaki, A., Nakato, A., Nishimura, M., Okada, T., Yada, T., Yogata, K., Nakazawa, S., Saiki, T., Tanaka, S., Terui, F., Tsuda, Y., Watanabe, S., Yoshikawa, M., Tachibana, S., Yurimoto, H., 2022. Ryugu's nucleosynthetic heritage from the outskirts of the Solar System. Sci. Adv. 8, eadd8141.

Horan, M.F., Carlson, R.W., Blichert-Toft, J., 2012. Pd–Ag chronology of volatile depletion, crystallization and shock in the muonionalusta IVA iron meteorite and implications for its parent body. Earth Planet. Sci. Lett. 351–352, 215–222.

Humbert, F., Libourel, G., France-Lanord, C., Zimmermann, L., Marty, B., 2000. CO_2-laser extraction-static mass spectrometry analysis of ultra-low concentrations of nitrogen in silicates. Geostand. Newslett. 24, 255–260.

Injerd, W.G., Kaplan, I.R., 1974. Nitrogen isotope distribution in meteorites. Meteoritics 9, 352–353.

Kakkenpara, S.S., Dulieu, F., Vitorino, J., Caselli, P., 2024. Experimental study of the binding energy of NH_3 on different types of ice and its impact on the snow line of NH_3 and H_2O. A&A 682, A163.

Kelly, W.R., Larimer, J.W., 1977. Chemical fractionations in meteorites—VIII. Iron meteorites and the cosmochemical history of the metal phase. Geochim. Cosmochim. Acta 41, 93–111.

Kerridge, J.F., 1985. Carbon, hydrogen and nitrogen in carbonaceous chondrites: abundances and isotopic compositions in bulk samples. Geochim. Cosmochim. Acta 49, 1707–1714.

Kothari, B.K., Goel, P.S., 1974. Total nitrogen in meteorites. Geochim. Cosmochim. Acta 38, 1493–1507.

Kress, M.E., Tielens, A.G.G.M., Frenklach, M., 2010. The 'soot line': destruction of presolar polycyclic aromatic hydrocarbon in the terrestrial planet-forming region of the disk. Adv. Space Res. 44, 44–49.

Krot, A.N., Amelin, Y., Cassen, P., Meibom, A., 2005. Young chondrules in CB chondrites from a giant impact in the early Solar System. Nature 435, 989–992.

Kruczkiewicz, F., Vitorino, J., Congiu, E., Theulé, P., Dulieu, F., 2021. Ammonia snow lines and ammonium salts desorption. Astron. Astroph. 652, A29.

Kruijer, T.S., Burkhardt, C., Budde, G., Kleine, T., 2017. Age of Jupiter inferred from the distinct genetics and formation times of meteorites. PNAS 114, 6712–6716.
Kung, C.C., Clayton, R.N., 1978. Nitrogen abundances and isotopic compositions in stony meteorites. Earth Planet. Sci. Lett. 38, 421–435.
Laize-Générat, L., Soussaintjean, L., Poch, O., Bonal, L., Savarino, J., Caillon, N., Ginot, P., Vella, A., Lamothe, A., Elazzouzi, R., Flandinet, L., Vacher, L., Gounelle, M., Bizarro, M., Beck, P., Quirico, E., Schmitt, B., 2024. Nitrogen in the Orgueil meteorite: abundant ammonium among other reservoirs of variable isotopic compositions. Geochim. Cosmochim. Acta 387, 111–129.
Lauretta, D.S., Connolly, H.C., Aebersold, J.E., Alexander, C.M.O'D., Ballouz, R., Barnes, J.J., Bates, H.C., Bennett, C.A., Blanche, L., Blumenfeld, E.H., Clemett, S.J., Cody, G.D., DellaGiustina, D.N., Dworkin, J.P., Eckley, S.A., Foustoukos, D.I., Franchi, I.A., Glavin, D.P., Greenwood, R.C., Haenecour, P., Hamilton, V.E., Hill, D. H., Hiroi, T., Ishimaru, K., Jourdan, F., Kaplan, H.H., Keller, L.P., King, A.J., Koefoed, P., Kontogiannis, M.K., Le, L., Macke, R.J., McCoy, T.J., Milliken, R.E., Najorka, J., Nguyen, A.N., Pajola, M., Polit, A.T., Righter, K., Roper, H.L., Russell, S. S., Ryan, A.J., Sandford, S.A., Schofield, P.F., Schultz, C.D., Seifert, L.B., Tachibana, S., Thomas-Keprta, K.L., Thompson, M.S., Tu, V., Tusberti, F., Wang, K., Zega, T.J., Wolner, C.W.V., OSIRIS-REx Sample Analysis Team, 2024. Asteroid (101955) Bennu in the laboratory: properties of the sample collected by OSIRIS-REx. Meteorit & Planetary Scien 59, 2453–2486.
Leitner, J., Vollmer, C., Henkel, T., Ott, U., Hoppe, P., 2018. An isotopic, elemental and structural study of silicon nitride from enstatite chondrites. Geochim. Cosmochim. Acta 235, 153–172.
Leitner, J., Vollmer, C., Hoppe, P., Zipfel, J., 2012. Characterization of presolar material in the CR chondrite Northwest Africa 852. ApJ 745, 38.
Lewis, C.F., Moore, C.B., 1970. Chemical analysis of thirty-eight iron meteorites. Meteoritics 195–205.
Lewis, R.S., Anders, E., Wright, I.P., Norris, S.J., Pillinger, C.T., 1983. Isotopically anomalous nitrogen in primitive meteorites. Nature 305, 767–771.
Li, J., Bergin, E.A., Blake, G.A., Ciesla, F.J., Hirschmann, M.M., 2021. Earth's carbon deficit caused by early loss through irreversible sublimation. Sci. Adv. 7, eabd3632.
Li, Y., Marty, B., Shcheka, S., Zimmermann, L., Keppler, H., 2016. Nitrogen isotope fractionation during terrestrial core-mantle separation. Geochem. Persp. Let. 2, 138–147.
Lodders, K., 2004. Jupiter formed with more tar than ice. ApJ 611, 587–597.
Luais, B., 2012. Germanium chemistry and MC-ICPMS isotopic measurements of Fe–Ni, Zn alloys and silicate matrices: insights into deep Earth processes. Chem. Geol. 334, 295–311.
Luais, B., 2007. Isotopic fractionation of germanium in iron meteorites: significance for nebular condensation, core formation and impact processes. Earth Planet. Sci. Lett. 262, 21–36.
Ma, N., Neumann, W., Néri, A., Schwarz, W.H., Ludwig, T., Trieloff, M., Klahr, H., Bouvier, A., 2022. Early formation of primitive achondrites in an outer region of the protoplanetary disc. Geochem. Persp. Let. 23, 33–37.
Marrocchi, Y., Füri, E., Zimmermann, L., Piani, L., 2026. H–N budgets and isotopic signatures of oued chebeika 002 and CI reservoir heterogeneity. Geochem. Persp. Let. 39, 7–11.
Marrocchi, Y., Piralla, M., Regnault, M., Batanova, V., Villeneuve, J., Jacquet, E., 2022. Isotopic evidence for two chondrule generations in CR chondrites and their relationships to other carbonaceous chondrites. Earth Planet. Sci. Lett. 593, 117683.
Marrocchi, Y., Avice, G., Barrat, J.-A., 2021. The Tarda meteorite: a window into the formation of D-type asteroids. ApJL 913, L9.
Marty, B., Zimmermann, L., Füri, E., Bekaert, D.V., Barnes, J.J., Nguyen, A.N., Connolly, H.C., Lauretta, D.S., 2025. Noble gases and nitrogen in material from asteroid Bennu. Meteorit. Planet Sci.
Marty, B., Chaussidon, M., Wiens, R.C., Jurewicz, A.J.G., Burnett, D.S., 2011. A ^{15}N-poor isotopic composition for the solar system as shown by genesis solar wind samples. Science 332, 1533–1536.
Marty, B., Kelley, S., Turner, G., 2010. Chronology and shock history of the Bencubbin meteorite: a nitrogen, noble gas, and Ar-Ar investigation of silicates, metal and fluid inclusions. Meteorit. Planet Sci.
Mathew, K.J., Murty, S.V.S., 1993. Cosmic ray produced nitrogen in extra terrestrial matter. Proc. Indian Natl. Sci. Acad. 102, 415–437.
Mathew, K.J., Palma, R.L., Marti, K., Lavielle, B., 2000. Isotopic signatures and origin of nitrogen in IIE and IVA iron meteorites. Geochim. Cosmochim. Acta 64, 545–557.
Matthes, M., Fischer-Gödde, M., Kruijer, T.S., Kleine, T., 2018. Pd-Ag chronometry of IVA iron meteorites and the crystallization and cooling of a protoplanetary core. Geochim. Cosmochim. Acta 220, 82–95.
McCoy, T.J., Walker, R.J., Goldstein, J.I., Yang, J., McDonough, W.F., Rumble, D., Chabot, N.L., Ash, R.D., Corrigan, C.M., Michael, J.R., Kotula, P.G., 2011. Group IVA irons: new constraints on the crystallization and cooling history of an asteroidal core with a complex history. Geochim. Cosmochim. Acta 75, 6821–6843.
Mittlefehldt, D.W., McCoy, T.J., Goodrich, C.A., Kracher A., 1998. Non-chondritic meteorites from asteroidal bodies. In: Planetary Materials (ed. Papike J. J.). Rev. Mineral. Geochem. **36**, 4-01-4-196.
Moore, C.B., Lewis, C.F., Nava, D., 1969. Superior analyses of iron meteorites. In: Millman, P.M. (Ed.), Meteorite Research, Astrophysics and Space Science Library. Springer, Dordrecht, pp. 738–748.
Murty, S.V.S., Marti, K., 1994. Nitrogen isotopic signatures in Cape York: implications for formation of Group III A irons. Geochim. Cosmochim. Acta 58, 1841–1848.
Murty, S.V.S., Ghosh, S., Ray, D., 2019. Noble gases and nitrogen in Raghunathpura (IIAB) and Nyaung (IIIAB) iron meteorites. Meteorit. Planet. Sci. 54, 90–103.
Murty, S.V.S., Goel, P.S., Minh, D.V., Shukolyukov, Y.A., 1983. Nitrogen and xenon in acid residues of iron meteorites. Geochim. Cosmochim. Acta 47, 1061–1068.
Nakamura, E., Kobayashi, K., Tanaka, R., Kunihiro, T., Kitagawa, H., Potiszil, C., Ota, T., Sakaguchi, C., Yamanaka, M., Ratnayake, D.M., Tripathi, H., Kumar, R., Avramescu, M.-L., Tsuchida, H., Yachi, Y., Miura, H., Abe, M., Fukai, R., Furuya, S., Hatakeda, K., Hayashi, T., Hitomi, Y., Kumagai, K., Miyazaki, A., Nakato, A., Nishimura, M., Okada, T., Soejima, H., Sugita, S., Suzuki, A., Usui, T., Yada, T., Yamamoto, D., Yogata, K., Yoshitake, M., Arakawa, M., Fujii, A., Hayakawa, M., Naoyuki, H., Naru, H., Honda, R., Honda, C., Hosoda, S., Iijima, Y., Ikeda, H., Ishiguro, M., Ishihara, Y., Iwata, T., Kawahara, K., Kikuchi, S., Kitazato, K., Matsumoto, K., Matsuoka, M., Michikami, T., Mimasu, Y., Miura, A., Morota, T., Nakazawa, S., Namiki, N., Noda, H., Noguchi, R., Ogawa, N., Ogawa, K., Okamoto, C., Ono, G., Ozaki, M., Saiki, T., Sakatani, N., Sawada, H., Senshu, H., Shimaki, Y., Shirai, K., Takei, Y., Takeuchi, H., Tanaka, S., Tatsumi, E., Terui, F., Tsukizaki, R., Wada, K., Yamada, M., Yamada, T., Yamamoto, Y., Yano, H., Yokota, Y., Yoshihara, K., Yoshikawa, M., Yoshikawa, K., Fujimoto, M., Watanabe, S., Tsuda, Y., 2022. On the origin and evolution of the asteroid Ryugu: a comprehensive geochemical perspective. Proc. Jpn. Acad Ser. B 98, 227–282.
Nakano, H., Kouchi, A., Tachibana, S., Tsuchiyama, A., 2003. Evaporation of interstellar organic materials in the solar nebula. ApJ 592, 1252–1262.
Nanne, J.A.M., Nimmo, F., Cuzzi, J.N., Kleine, T., Abbott, D.A., Burgess, L., Longhi, J., Smith, W.H.F., 2019. Origin of the non-carbonaceous–carbonaceous meteorite dichotomy. Earth Planet. Sci. Lett. 511, 44–54.
Naraoka, H., Takano, Y., Dworkin, J.P., Oba, Y., Hamase, K., Furusho, A., Ogawa, N.O., Hashiguchi, M., Fukushima, K., Aoki, D., Schmitt-Kopplin, P., Aponte, J.C., Parker, E.T., Glavin, D.P., McLain, H.L., Elsila, J.E., Graham, H.V., Eiler, J.M., Orthous-Daunay, F.-R., Wolters, C., Isa, J., Vuitton, V., Thissen, R., Sakai, S., Yoshimura, T., Koga, T., Ohkouchi, N., Chikaraishi, Y., Sugahara, H., Mita, H., Furukawa, Y., Hertkorn, N., Ruf, A., Yurimoto, H., Nakamura, T., Noguchi, T., Okazaki, R., Yabuta, H., Sakamoto, K., Tachibana, S., Connolly, H.C., Lauretta, D.S., Abe, M., Yada, T., Nishimura, M., Yogata, K., Nakato, A., Yoshitake, M., Suzuki, A., Miyazaki, A., Furuya, S., Hatakeda, K., Soejima, H., Hitomi, Y., Kumagai, K., Usui, T., Hayashi, T., Yamamoto, D., Fukai, R., Kitazato, K., Sugita, S., Namiki, N., Arakawa, M., Ikeda, H., Ishiguro, M., Naru, H., Wada, K., Ishihara, Y., Noguchi, R., Morota, T., Sakatani, N., Matsumoto, K., Senshu, H., Honda, R., Tatsumi, E., Yokota, Y., Honda, C., Michikami, T., Matsuoka, M., Miura, A., Noda, H., Yamada, T., Yoshihara, K., Kawahara, K., Ozaki, M., Iijima, Y., Yano, H., Hayakawa, M., Iwata, T., Tsukizaki, R., Sawada, H., Hosoda, S., Ogawa, K., Okamoto, C., Naoyuki, H., Shirai, K., Shimaki, Y., Yamada, M., Okada, T., Yamamoto, Y., Takeuchi, H., Fujii, A., Takei, Y., Yoshikawa, K., Mimasu, Y., Ono, G., Ogawa, N., Kikuchi, S., Nakazawa, S., Terui, F., Tanaka, S., Saiki, T., Yoshikawa, M., Watanabe, S., Tsuda, Y., 2023. Soluble organic molecules in samples of the carbonaceous asteroid (162173) Ryugu. Science 379, eabn9033.
Nash, L.K., Baxter, G.P., 1947. The determination of the gases in meteoritic and terrestrial irons and steels. J. Am. Chem. Soc. 69, 2534–2544.
Neumann, W., Ma, N., Bouvier, A., Trieloff, M., 2024. Recurrent planetesimal formation in an outer part of the early solar system. Sci. Rep. 14.
Nielsen, H.P., Buchwald, V.F., 1981. Roaldite, a new nitride in iron meteorites. Proc. 12th Lunar Planet. Sci. Conf., 1343–1348.
Nier, A., 1950. A redetermination of the relative abundances of the isotopes of carbon, nitrogen, oxygen, argon, and potassium. Phys. Rev. 77, 789–793.
Oba, Y., Koga, T., Takano, Y., Ogawa, N.O., Ohkouchi, N., Sasaki, K., Sato, H., Glavin, D. P., Dworkin, J.P., Naraoka, H., Tachibana, S., Yurimoto, H., Nakamura, T., Noguchi, T., Okazaki, R., Yabuta, H., Sakamoto, K., Yada, T., Nishimura, M., Nakato, A., Miyazaki, A., Yogata, K., Abe, M., Okada, T., Usui, T., Yoshikawa, M., Saiki, T., Tanaka, S., Terui, F., Nakazawa, S., Watanabe, S., Tsuda, Y., 2023. Hayabusa2-initial-analysis SOM team, uracil in the carbonaceous asteroid (162173) Ryugu. Nat. Commun. 14, 1292.
Oberg, N., Cazaux, S., Kamp, I., Bründl, T.-M., Thi, W.F., Immerzeel, C., 2023. Circumplanetary disk ices: II. Composition. Astron. Astroph. 672, A142.
Oka, A., Nakamoto, T., Ida, S., 2011. Evolution of snow line in optically thick protoplanetary disks: effects of water ice opacity and dust grain size. ApJ 738, 141.
Okazaki, R., Marty, B., Busemann, H., Hashizume, K., Gilmour, J.D., Meshik, A., Yada, T., Kitajima, F., Broadley, M.W., Byrne, D., Füri, E., Riebe, M.E.I., Krietsch, D., Maden, C., Ishida, A., Clay, P., Crowther, S.A., Fawcett, L., Lawton, T., Pravdivtseva, O., Miura, Y.N., Park, J., Bajo, K., Takano, Y., Yamada, K., Kawagucci, S., Matsui, Y., Yamamoto, M., Righter, K., Sakai, S., Iwata, N., Shirai, N., Sekimoto, S., Inagaki, M., Ebihara, M., Yokochi, R., Nishiizumi, K., Nagao, K., Lee, J. I., Kano, A., Caffee, M.W., Uemura, R., Nakamura, T., Naraoka, H., Noguchi, T., Yabuta, H., Yurimoto, H., Tachibana, S., Sawada, H., Sakamoto, K., Abe, M., Arakawa, M., Fujii, A., Hayakawa, M., Naoyuki, H., Naru, H., Honda, R., Honda, C., Hosoda, S., Iijima, Y., Ikeda, H., Ishiguro, M., Ishihara, Y., Iwata, T., Kawahara, K., Kikuchi, S., Kitazato, K., Matsumoto, K., Matsuoka, M., Michikami, T., Mimasu, Y., Miura, A., Morota, T., Nakazawa, S., Namiki, N., Noda, H., Noguchi, R., Ogawa, N., Ogawa, K., Okada, T., Okamoto, C., Ono, G., Ozaki, M., Saiki, T., Sakatani, N., Senshu, H., Shimaki, Y., Shirai, K., Sugita, S., Takei, Y., Takeuchi, H., Tanaka, S., Tatsumi, E., Terui, F., Tsukizaki, R., Wada, K., Yamada, M., Yamada, T., Yamamoto, Y., Yano, H., Yokota, Y., Yoshihara, K., Yoshikawa, M., Yoshikawa, K., Furuya, S., Hatakeda, K., Hayashi, T., Hitomi, Y., Kumagai, K., Miyazaki, A., Nakato, A., Nishimura, M., Soejima, H., Iwamae, A., Yamamoto, D., Yogata, K., Yoshitake, M., Fukai, R., Usui, T., Connolly, H.C., Lauretta, D., Watanabe, S., Tsuda, Y., 2023. Noble gases and nitrogen in samples of asteroid Ryugu record its volatile sources and recent surface evolution. Science 379, eabo0431.
Ott, U., 2014. Planetary and pre-solar noble gases in meteorites. Chem. Erde. - Geochem. 74, 519–544.
Pathak, D., Dasgupta, R., 2024. Nitrogen inventory of iron meteorite parent bodies constrained by nitrogen partitioning between Fe-rich solid and liquid alloys. Geochim. Cosmochim. Acta 371, 199–213.

Patzek, M., Kadlag, Y., Rüfenacht, M., Füri, E., Pack, A., Bischoff, A., Becker, H., Visser, R., John, T., Schönbächler, M., 2025. Multi-isotope (N, O, Ti, and Cr) study of C1 and CM-like clasts—probing unsampled C1 material. Meteorit. Planet. Sci. 60, 1073–1094.

Pearson, V.K., Sephton, M.A., Franchi, I.A., Gibson, J.M., Gilmour, I., 2006. Carbon and nitrogen in carbonaceous chondrites: elemental abundances and stable isotopic compositions. Meteorit. Planet. Sci. 41, 1899–1918.

Pepin, R.O., Becker, R.H., 1982. Nitrogen isotopes in iron meteorites. Meteoritics 17, 269–274.

Piani, L., Marrocchi, Y., Vacher, L.G., Yurimoto, H., Bizzarro, M., 2021. Origin of hydrogen isotopic variations in chondritic water and organics. Earth Planet. Sci. Lett. 567, 117008.

Piso, A.-M.-A., Pegues, J., Öberg, K.I., 2016. The role of ice compositions for snowlines and the C/N/O ratios in active disks. ApJ 833, 203.

Pizzarello, S., Williams, L.B., 2012. Ammonia in the early solar system: an account from carbonaceous meteorites. ApJ 749, 161.

Poch, O., Istiqomah, I., Quirico, E., Beck, P., Schmitt, B., Theulé, P., Faure, A., Hily-Blant, P., Bonal, L., Raponi, A., Ciarniello, M., Rousseau, B., Potin, S., Brissaud, O., Flandinet, L., Filacchione, G., Pommerol, A., Thomas, N., Kappel, D., Mennella, V., Moroz, L., Vinogradoff, V., Arnold, G., Erard, S., Bockelée-Morvan, D., Leyrat, C., Capaccioni, F., De Sanctis, M.C., Longobardo, A., Mancarella, F., Palomba, E., Tosi, F., 2020. Ammonium salts are a reservoir of nitrogen on a cometary nucleus and possibly on some asteroids. Science 367, eaaw7462.

Ponganis, K.V., Marti, K., 2007. Nitrogen components in IAB/IIICD iron meteorites. Meteorit. Planet. Sci. 42, 331–346.

Preston, H.L., 1903. Reed city meteorite. J. Geol. 11, 230–233.

Prombo, C.A., Clayton, R.N., 1993. Nitrogen isotopic compositions of iron meteorites. Geochim. Cosmochim. Acta 57, 3749–3761.

Rasmussen, K.L., Malvin, D.J., Buchwald, V.F., Wasson, J.T., 1984. Compositional trends and cooling rates of group IVB iron meteorites. Geochim. Cosmochim. Acta 48, 805–813.

Reedy, R.C., 1981. Cosmic-ray produced stable nuclides: various production rates and their implications. Proc. 12th Lunar Planet. Sci. Conf., 1809–1823.

Remusat, L., Bonnet, J.-Y., Bernard, S., Buch, A., Quirico, E., 2019. Molecular and isotopic behavior of insoluble organic matter of the Orgueil meteorite upon heating. Geochim. Cosmochim. Acta 263.

Righter, K., Sutton, S.R., Danielson, L., Pando, K., Newville, M., 2016. Redox variations in the inner solar system with new constraints from vanadium XANES in spinels. Am. Mineral. 101, 1928–1942.

Rivkin, A.S., Emery, J.P., Howell, E.S., Kareta, T., Noonan, J.W., Richardson, M., Sharkey, B.N.L., Sickafoose, A.A., Woodney, L.M., Cartwright, R.J., Lindsay, S., Mcclure, L.T., 2022. The nature of low-albedo small bodies from 3 μm spectroscopy: one group that formed within the ammonia snow line and one that formed beyond it. Planet. Sci. J. 3, 153.

Robert, F., Epstein, S., 1982. The concentration and isotopic composition of hydrogen, carbon and nitrogen in carbonaceous meteorites. Geochim. Cosmochim. Acta 46, 81–95.

Rubin, A.E., 2018. Carbonaceous and noncarbonaceous iron meteorites: differences in chemical, physical, and collective properties. Meteorit. Planet. Sci. 53, 2357–2371.

Rubin, A.E., 2011. Origin of the differences in refractory-lithophile-element abundances among chondrite groups. Icarus 213, 547–558.

Rubin, A.E., 1997. Mineralogy of meteorite groups. Meteorit. Planet. Sci. 32, 231–247.

Rubin, A.E., Jerde, E.A., Zong, P., Wasson, J.T., Westcott, J.W., Mayeda, T.K., Clayton, R. N., 1986. Properties of the Guin ungrouped iron meteorite: the origin of Guin and of group-IIE irons. Earth Planet. Sci. Lett. 76, 209–226.

Ruzicka, A., Hutson, M., 2006. Differentiation and evolution of the IVA meteorite parent body: clues from pyroxene geochemistry in the Steinbach stony-iron meteorite. Meteorit. Planet. Sci. 41, 1959–1987.

Sanborn, M.E., Wimpenny, J., Williams, C.D., Yamakawa, A., Amelin, Y., Irving, A.J., Yin, Q.-Z., 2019. Carbonaceous achondrites Northwest Africa 6704/6693: milestones for early Solar System chronology and genealogy. Geochim. Cosmochim. Acta 245, 577–596.

Saxton, J.M., 2020. The $^{21}Ne/^{20}Ne$ ratio of atmospheric neon. J. Anal. At. Spectrom 35, 943–952.

Schrader, D.L., Nagashima, K., Krot, A.N., Ogliore, R.C., Yin, Q.-Z., Amelin, Y., Stirling, C.H., Kaltenbach, A., 2017. Distribution of ^{26}Al in the CR chondrite chondrule-forming region of the protoplanetary disk. Geochim. Cosmochim. Acta 201, 275–302.

Scott, E.R.D., 2020. Iron meteorites: composition, age, and origin. Oxford Research Encyclopedia of Planetary Science.

Scott, E.R.D., 1972. Chemical fractionation in iron meteorites. Geochim. Cosmochim. Acta 36, 1205–1236.

Scott, E.R.D., Wasson, J.T., 1975. Classification and properties of iron meteorites. Rev. Geophys. 13, 527–546.

Sears, D.W., 1978. Condensation and the composition of iron meteorites. Earth Planet. Sci. Lett. 41, 128–138.

Sephton, M.A., Verchovsky, A.B., Bland, P.A., Gilmour, I., Grady, M.M., Wright, I.P., 2003. Investigating the variations in carbon and nitrogen isotopes in carbonaceous chondrites. Geochim. Cosmochim. Acta 67, 2093–2108.

Shi, L., Lu, W., Kagoshima, T., Sano, Y., Gao, Z., Du, Z., Liu, Y., Fei, Y., Li, Y., 2022. Nitrogen isotope evidence for Earth's heterogeneous accretion of volatiles. Nat. Commun. 13, 4769.

Shollenberger, Q.R., Render, J., Wimpenny, J., Armytage, R.M.G., Gunawardena, N., Rolison, J.M., Simon, J.I., Brennecka, G.A., 2025. Elemental and isotopic signatures of asteroid Ryugu support three early Solar System reservoirs. Earth Planet. Sci. Lett. 664, 119443.

Shukla, P.N., Goel, P.S., 1981. Total nitrogen in iron meteorites. Earth Planet. Sci. Lett. 52, 251–258.

Simon, A., Öberg, K.I., Rajappan, M., Maksiutenko, P., 2019. Entrapment of CO in CO_2 ice. Astroph. J 883, 21.

Singerling, S.A., Brearley, A.J., 2020. Altered primary iron sulfides in CM2 and CR2 carbonaceous chondrites: insights into parent body processes. Meteorit. Planet. Sci. 55, 496–523.

Spitzer, F., Burkhardt, C., Kruijer, T.S., Kleine, T., 2025a. Comparison of the earliest NC and CC planetesimals: evidence from ungrouped iron meteorites. Geochim. Cosmochim. Acta 397, 134–148.

Spitzer, F., Hopp, T., Burkhardt, C., Dauphas, N., Kleine, T., 2025b. The evolution of planetesimal reservoirs revealed by Fe-Ni isotope anomalies in differentiated meteorites. Earth Planet. Sci. Lett. 667, 119530.

Spitzer, F., Kleine, T., Burkhardt, C., Hopp, T., Yokoyama, T., Abe, Y., Aléon, J.O'D., Alexander, C.M.O'D., Amari, S., Amelin, Y., Bajo, K., Bizzarro, M., Bouvier, A., Carlson, R.W., Chaussidon, M., Choi, B.-G., Dauphas, N., Davis, A.M., Di Rocco, T., Fujiya, W., Fukai, R., Gautam, I., Haba, M.K., Hibiya, Y., Hidaka, H., Homma, H., Hoppe, P., Huss, G.R., Ichida, K., Iizuka, T., Ireland, T.R., Ishikawa, A., Itoh, S., Kawasaki, N., Kita, N.T., Kitajima, K., Komatani, S., Krot, A.N., Liu, M.-C., Masuda, Y., Morita, M., Moynier, F., Motomura, K., Nakai, I., Nagashima, K., Nguyen, A., Nittler, L., Onose, M., Pack, A., Park, C., Piani, L., Qin, L., Russell, S.S., Sakamoto, N., Schönbächler, M., Tafla, L., Tang, H., Terada, K., Terada, Y., Usui, T., Wada, S., Wadhwa, M., Walker, R.J., Yamashita, K., Yin, Q.-Z., Yoneda, S., Young, E. D., Yui, H., Zhang, A.-C., Nakamura, T., Naraoka, H., Noguchi, T., Okazaki, R., Sakamoto, K., Yabuta, H., Abe, M., Miyazaki, A., Nakato, A., Nishimura, M., Okada, T., Yada, T., Yogata, K., Nakazawa, S., Saiki, T., Tanaka, S., Terui, F., Tsuda, Y., Watanabe, S., Yoshikawa, M., Tachibana, S., Yurimoto, H., 2024. The Ni isotopic composition of Ryugu reveals a common accretion region for carbonaceous chondrites. Sci. Adv. 10, eadp2426.

Spitzer, F., Burkhardt, C., Pape, J., Kleine, T., 2022. Collisional mixing between inner and outer solar system planetesimals inferred from the Nedagolla iron meteorite. Meteorit. Planet. Sci. 57, 261–276.

Spitzer, F., Burkhardt, C., Nimmo, F., Kleine, T., 2021. Nucleosynthetic Pt isotope anomalies and the Hf-W chronology of core formation in inner and outer solar system planetesimals. Earth Planet. Sci Lett. 576.

Spitzer, F., Burkhardt, C., Budde, G., Kruijer, T.S., Morbidelli, A., Kleine, T., 2020. Isotopic evolution of the inner Solar System inferred from molybdenum isotopes in meteorites. Astroph. J. 898, L2.

Sridhar, S., Bryson, J.F.J., King, A.J., Harrison, R.J., 2021. Constraints on the ice composition of carbonaceous chondrites from their magnetic mineralogy. Earth Planet. Sci. Lett. 576, 117243.

Sugiura, N., 1998. Ion probe measurements of carbon and nitrogen in iron meteorites. Meteorit. Planet. Sci. 33, 393–409.

Sugiura, N., Zashu, S., 1993. Isotopic composition of nitrogen in the PCA 91002 R group chondrite. Proc. 8th Symp. Antarct. Meteorites, Mem. Natl. Inst. Polar Res. 8, 273–285.

Sugiura, N., Ikeda, Y., Zashu, S., Wasson, J.T., 2000. Nitrogen-isotopic compositions of IIIE iron meteorites. Meteorit. Planet. Sci. 35, 749–756.

Sugiura, N., Kiyota, K., Hashizume, K., 1998. Nitrogen components in primitive ordinary chondrites. Meteorit. Planet. Sci. 33, 463–482.

Tenner, T.J., Nakashima, D., Ushikubo, T., Tomioka, N., Kimura, M., Weisberg, M.K., Kita, N.T., 2019. Extended chondrule formation intervals in distinct physicochemical environments: evidence from Al-Mg isotope systematics of CR chondrite chondrules with unaltered plagioclase. Geochim. Cosmochim. Acta 260, 133–160.

Thiemens, M.H., Clayton, R.N., 1981. Nitrogen isotopes in the allende meteorite. Earth Planet. Sci. Lett. 55, 363–369.

Thiemens, M.H., Clayton, R.N., 1983. Nitrogen contents and isotopic ratios of clasts from the enstatite chondrite abee. Earth Planet. Sci. Lett. 62, 165–168.

Tissot, F.L.H., Burkhardt, C., Kuznetsova, A., Pack, A., Schiller, M., Spitzer, F., Van Kooten, E., Yap, T.E., 2025. Infall and disk processes – the message from meteorites. Space Sci. Rev. 221, 85.

Trinquier, A., Elliott, T., Ulfbeck, D., Coath, C., Krot, A.N., Bizzarro, M., 2009. Origin of nucleosynthetic isotope heterogeneity in the solar protoplanetary disk. Science 324, 374–376.

Trinquier, A., Birck, J., Allegre, C.J., 2007. Widespread ^{54}Cr heterogeneity in the inner Solar System. ApJ 655, 1179–1185.

Vacher, L.G., Eschrig, J., Bonal, L., Fujiya, W., Flandinet, L., Beck, P., 2025. Thermal metamorphism and volatile evolution in unequilibrated ordinary chondrites: implications for the delivery of hydrogen to terrestrial planets. Geochim. Cosmochim. Acta 391, 106–126.

Vacher, L.G., Piani, L., Rigaudier, T., Thomassin, D., Florin, G., Piralla, M., Marrocchi, Y., 2020. Hydrogen in chondrites: influence of parent body alteration and atmospheric contamination on primordial components. Geochim. Cosmochim. Acta 281, 53–66.

Van Kooten, E., Zhao, X., Franchi, I., Tung, P.-Y., Fairclough, S., Walmsley, J., Onyett, I., Schiller, M., Bizzarro, M., 2024. The nucleosynthetic fingerprint of the outermost protoplanetary disk and early Solar System dynamics. Sci. Adv. 10, eadp1613.

Vogt, M., Trieloff, M., Ott, U., Hopp, J., Schwarz, W.H., 2021. Solar noble gases in an iron meteorite indicate terrestrial mantle signatures derive from Earth's core. Commun. Earth Environ. 2, 1–8.

Voshage, H., Feldmann, H., 1979. Investigations on cosmic-ray-produced nuclides in iron meteorites, 3. Exposure ages, meteoroid sizes and sample depths determined by mass spectrometric analyses of potassium and rare gases. Earth Planet. Sci. Lett. 45, 293–308.

Warren, P.H., 2011. Stable-isotopic anomalies and the accretionary assemblage of the Earth and Mars: a subordinate role for carbonaceous chondrites. Earth Planet. Sci. Lett. 311, 93–100.

Wasson, J.T., 2011. Relationship between iron-meteorite composition and size: compositional distribution of irons from North Africa. Geochim. Cosmochim. Acta 75, 1757–1772.

Wasson, J.T., 1970. The chemical classification of iron meteorites. IV. Irons with Ge concentrations greater than 190 ppm and other meteorites associated with group I. Icarus 12, 407–423.

Wasson, J.T., 1969. The chemical classification of iron meteorites-III. Hexahedrites and other irons with germanium concentrations between 80 and 200 ppm. Geochim. Cosmochim. Acta 33.

Wasson, J.T., 1967. The chemical classification of iron meteorites: I. A study of iron meteorites with low concentrations of gallium and germanium. Geochim. Cosmochim. Acta 31, 161–180.

Wasson, J.T., Choe, W.-H., 2009. The IIG iron meteorites: probable formation in the IIAB core. Geochim. Cosmochim. Acta 73, 4879–4890.

Wasson, J.T., Huber, H., 2006. Compositional trends among IID irons; their possible formation from the P-rich lower magma in a two-layer core. Geochim. Cosmochim. Acta 70, 6153–6167.

Wasson, J.T., Kimbeblin, J., 1967. The chemical classification of iron meteorites-II. Irons and pallasites with germanium concentrations between 8 and 100 ppm. Geochim. Cosmochim. Acta 31.

Wasson, J.T., Huber, H., Malvin, D.J., 2007. Formation of IIAB iron meteorites. Geochim. Cosmochim. Acta 71, 760–781.

Wasson, J.T., Matsunami, Y., Rubin, A.E., 2006. Silica and pyroxene in IVA irons; possible formation of the IVA magma by impact melting and reduction of L-LL-chondrite materials followed by crystallization and cooling. Geochim. Cosmochim. Acta 70, 3149–3172.

Wielandt, D., Storey, M., 2019. A new high precision determination of the atmospheric ^{21}Ne abundance. J. Anal. At. Spectrom 34, 535–549.

Wriedt, H.A., Gonzalez, O.D., 1961. The solubility of nitrogen in solid iron-nickel alloys near 1000°C. Trans. Metall. Soc. AIME 221, 532–535.

Yang, J., Goldstein, J.I., 2005. The formation of the Widmanstätten structure in meteorites. Meteorit. Planet. Sci. 40, 239–253.

Yang, L., Ciesla, F.J., Alexander, C.M., O'd., 2013. The D/H ratio of water in the solar nebula during its formation and evolution. Icarus 226, 256–267.

Yang, J., Goldstein, J.I., Scott, E.R.D., Michael, J.R., Kotula, P.G., Pham, T., McCOY, T.J., 2011. Thermal and impact histories of reheated group IVA, IVB, and ungrouped iron meteorites and their parent asteroids. Meteorit. Planet. Sci. 46, 1227–1252.

Yang, J., Goldstein, J.I., Scott, E.R.D., 2008. Metallographic cooling rates and origin of IVA iron meteorites. Geochim. Cosmochim. Acta 72, 3043–3061.

Yang, J., Goldstein, J.I., Scott, E.R.D., 2007. Iron meteorite evidence for early formation and catastrophic disruption of protoplanets. Nature 446, 888–891.

Zhang, B., Chabot, N.L., Rubin, A.E., 2024. Compositions of iron-meteorite parent bodies constrain the structure of the protoplanetary disk. PNAS 121, e2306995121.

Zhang, Z., Driscoll, P.E., 2025. Inefficient loss of moderately volatile elements from exposed planetesimal magma oceans. J. Geophys. Res. Planets 130, e2024JE008671.

Zimmermann, L., Füri, E., 2015. Purification des gaz rares sous ultravide - Enceinte de purification. Techniques de l'Ingénieur, J6634.

Zimmermann, L., Füri, E., Boulliung, J., Saxton, J., 2025. Performance of the 3F4M noblesse–HR noble gas mass spectrometer for multicollection Ne-Ar-N_2 analyses. Geochem. Geophys. Geosyst. 26, e2025GC012247.

Zimmermann, L., Füri, E., Burnard, P., 2015. Purification des gaz rares sous ultravide - méthodes de purification. Techniques De L'ingénieur J6635.